

Dwarf galaxies in the Dynamically Evolved NGC 1407 Group

Neil Trentham¹, R. Brent Tully² and Andisheh Mahdavi^{2,3}

¹ Institute of Astronomy, Madingley Road, Cambridge, CB3 0HA.

² Institute for Astronomy, University of Hawaii, 2680 Woodlawn Drive, Honolulu HI 96822, U. S. A.

³ Physics and Astronomy, University of Victoria, Victoria, BC V8W 3P6, Canada

16 May 2018

ABSTRACT

The NGC 1407 Group stands out among nearby structures by its properties that suggest it is massive and evolved. It shares properties with entities that have been called fossil groups: the 1.4^{mag} differential between the dominant elliptical galaxy and the second brightest galaxy comes close to satisfying the definition that has been used to define the fossil class. There are few intermediate luminosity galaxies, but a large number of dwarfs in the group. We estimate there are 250 group members to the depth of our survey. The slope of the faint end of the luminosity function (reaching $M_R = -12$) is $\alpha = -1.35$. Velocities for 35 galaxies demonstrate that this group with one dominant galaxy has a mass of $7 \times 10^{13} M_\odot$ and $M/L_R = 340 M_\odot/L_\odot$. Two galaxies in close proximity to NGC 1407 have very large blueshifts. The most notable is the second brightest galaxy, NGC 1400, with a velocity of -1072 km s^{-1} with respect to the group mean. We report the detection of X-ray emission from this galaxy and from the group.

Key words: galaxies: photometry – galaxies: clusters: individual: NGC 1407 Group – galaxies: luminosity function – galaxies: mass function

1 INTRODUCTION

This paper presents a continuation of a study of the dwarf galaxy populations in a variety of environments within the Local Supercluster (Trentham, Tully, & Verheijen 2001; Trentham & Tully 2002 [TT02]; Mahdavi, Trentham, & Tully 2005 [MTT05]). Our goals are to give better precision to the properties of the luminosity function of galaxies at faint levels and to determine the nature of any variations with environment.

Our earlier observations affirmed the claims of a deficiency of low-luminosity dwarf galaxies compared with the large number of low-mass dark-matter halos predicted by cold dark matter (CDM) theory (Klypin et al. 1999, Moore et al. 1999). The discrepancy is large – more than one order of magnitude – and potentially a problem for CDM theory. These studies also point towards a situation where there are more low-luminosity dwarf galaxies per high-luminosity giant galaxy in dense clusters than in the field. This discrepancy is much weaker: studies of the Virgo cluster (e.g. Trentham and Hodgkin 2002) showed that there are about twice as many dwarf galaxies per giant there than in the field. There is an upturn in the cluster luminosity function at $M_B = -16$ that is not seen in the field luminosity function. Interestingly this upturn has also been seen in a large

study of rich clusters using SDSS data (Popescu et al. 2005). The Virgo data is deep enough and the cluster is near enough that we can see the luminosity function begin to flatten again at about $M_B = -13$.

There are a number of physical processes during galaxy formation which could generate the observed phenomena. For example, the suppression of the formation of low-mass galaxies may be a strong function of the state of the intergalactic medium. At later times, after reionization, the intergalactic medium is too hot to permit the collapse of gas into any small dark-matter halos that may form. If gas must be cold to accumulate, there will be more dwarfs per giant in any part of the Universe where galaxies form early, for example, galaxy clusters. Another mechanism might be the pressure-confinement of gas within galaxies by an intracluster medium. This would reduce the feedback effects of supernova-driven winds in low-mass galaxies in galaxy clusters, where such a medium is present. Yet another mechanism would be the inability of giant galaxies to consume dwarfs in galaxy clusters, where the velocity dispersion is high.

Simulations of galaxy formation that investigate the roles of these different physical processes are limited by a lack of observational data, and it is this deficiency that our

study attempts to address. Our plan is to measure the galaxy luminosity function to faint limits in environments that have had different formation histories. The availability of large format digital detectors provides an opportunity to gather much better statistics on the occurrence of dwarf galaxies. The present study is based on observations with the Canada-France-Hawaii Telescope 12K detector, the predecessor of the current MegaCam CCD mosaic (Aune et al. 2003). The ultimate intention is to survey a representative sample of nearby groups and clusters that span wide ranges of density and mass. MTT05 presented results on the first region to be fully surveyed in our program, the intermediate mass but dense NGC 5846 Group.

Small, dense groups were observed earliest in the program for the practical reason that they subtend modest areas on the sky. More extended groups have subsequently been observed with the larger format MegaCam at CFHT and the results from these studies will follow. The current study concerns an unusual group in the context of the Local Supercluster region. The group of galaxies centered on NGC 1407 is sparse in luminous systems, but its velocity dispersion is high, and the group appears to be dynamically evolved. It shares the properties of ‘fossil’ groups (Ponman et al. 1994). It fails slightly to meet the formal qualification for such a group that there be a differential of at least 2 magnitudes between the brightest and second brightest objects since the interval between NGC 1407 and NGC 1400 is only 1.4 magnitudes. In any event, among structures with $V < 2,000 \text{ km s}^{-1}$ the NGC 1407 Group is extreme.

2 THE UNUSUAL NGC 1407 GROUP

This small group of E and S0 galaxies dominated by NGC 1407 has attracted attention because of a suspected high mass-to-light ratio M/L (Gould 1993; Quintana, Fouqué, and Way 1994). The group velocity dispersion based on 35 measurements is $387 \pm 65 \text{ km s}^{-1}$. The mass of the group found from application of the virial theorem is $7.3 \times 10^{13} M_{\odot}$. The mass-to-light ratio in the R band is then $M/L_R = 340 M_{\odot}/L_{\odot}$. Astonishingly, the second brightest galaxy in the group, NGC 1400, is *blueshifted* by 1072 km s^{-1} with respect to the group mean of 1630 km s^{-1} , a line-of-sight velocity excursion of 2.8σ . If the 3D velocity dispersion is proportional to the projected excursion and mass is distributed like the light, then 75 per cent of the orbital kinetic energy of the group would be attributed to this one galaxy. This circumstance is unlikely. The most plausible resolution is that most of the mass is in an extended group halo and that NGC 1400 is akin to a test particle of negligible mass, presently near the potential minimum and directed close to our line of sight. Surface brightness fluctuation measurements (Tonry et al. 2001) assure that NGC 1400 is indeed at the same distance as NGC 1407. Note that this reasonably direct inference that most of the group mass is decoupled from the light strongly negates the hypothesis of modified Newtonian gravity (Milgrom 1983).

The existence of groups with such high mass-to-light ratios is reasonable in the context of Λ CDM cosmology (see Gao et al. 2004 for a description of some of the important physical processes). That the group around NGC 1407 is an example of such a group comes mainly from dynamical

Table 1. Properties of the NGC 1407 Group

Designation*	51 – 8
Distance (Mpc)	25
No. E/S0/Sab $M_R < -19$	13
No. Sb-Irr $M_R < -19$	1
Velocity dispersion (km s^{-1})	387
Inertial radius (Mpc)	0.39
Crossing time	$0.07 H_0^{-1}$
$\text{Log}_{10} (R \text{ luminosity}/L_{\odot})$	11.33
$\text{Log}_{10} (\text{Mass}/M_{\odot})$	13.87
R band mass-to-light ratio / M_{\odot}/L_{\odot}	340
Density/Mpc ² at 200 kpc $M_R < -17$	34
Dwarfs / giants	6.5 ± 1.3

* This is the designation given in the *Nearby Galaxies Catalog* (Tully 1988).

evidence, of which the relative velocity of NGC 1407 and NGC 1400 is the most striking. Given that surface brightness fluctuations place these two early-type galaxies at the same distance, the probability of their *not* being bound is extremely small. Nevertheless, it is important to recognize the alternative (although we believe less likely) possibility that NGC 1400 has a high velocity relative to NGC 1407 because it is passing through the group, maybe for the first time.

The NGC 1407 Group resembles but is more extreme than the NGC 5846 Group discussed by MTT05. The NGC 5846 Group is a dumbbell system of $8 \times 10^{13} M_{\odot}$ arranged about two dominant ellipticals. The NGC 1407 Group has essentially as much mass but with a tighter concentration around the central large elliptical and an even greater predominance of early-type galaxies.

These characteristics lead us to identify the structure as akin to a “fossil group”, an entity at an advanced dynamical stage. After a search for small groups dominated by an elliptical at least 2 magnitudes brighter than any companion, Khosroshahi et al. (2004) identified the group around NGC 6482 at $V_{GSR} = 4089 \text{ km s}^{-1}$ as the nearest entity to satisfy the ‘fossil’ criterion. The NGC 1407 Group at $V_{GSR} = 1546 \text{ km s}^{-1}$ does not quite satisfy the magnitude differential criterion but it is the most extreme structure of a similar nature within 2000 km s^{-1} . Another difference between this group and fossil groups concerns large-scale environment; the NGC 1407 Group exists in a richer supercluster environment than most fossil groups. Given these differences it would not be correct to refer to this group as a fossil group. Nevertheless it is intriguing that such a nearby group shares so many properties with these rare objects.

2.1 The group environment

Before studying the group properties, we need to look in some detail at the region of sky around the group because of concerns regarding projection contamination. The NGC 1407 Group, 51-8 in the *Nearby Galaxies Catalog* (Tully 1988), is 18 degrees ($\sim 8 \text{ Mpc}$) away in projection from the Fornax Cluster (51-1). It is part of the Eridanus Cloud which contains other knots of early type systems in the vicinity. The extended region called 51-4 containing the

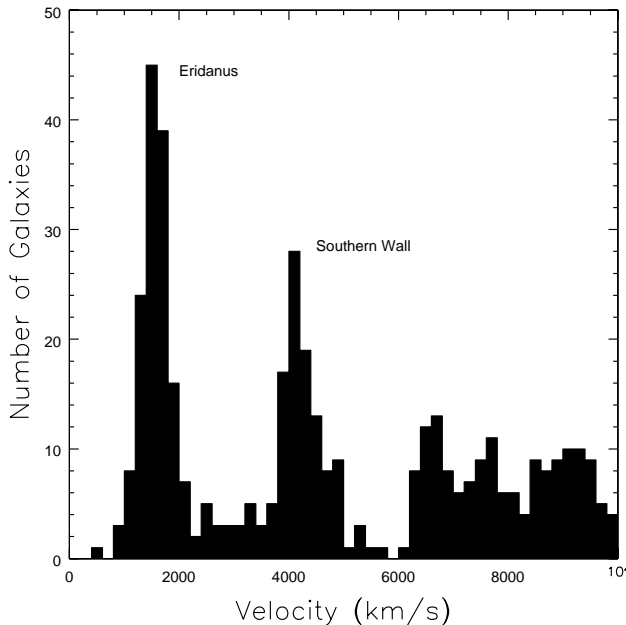


Figure 1. Histogram of velocities of galaxies projected onto the Eridanus region shown in Fig. 2.

dominant galaxies NGC 1332, 1371, 1395, and 1398 is 2–3 Mpc removed in projection and 300 km s^{−1} blueshifted in the mean. The Eridanus region excluding the NGC 1407 Group must contain at least $3 \times 10^{13} M_{\odot}$ (the combination of groups 51–4, 5, 7 in Table 1 of Tully 2005). Though the NGC 1407 Group appears distinct today it must be strongly suspected that the entire core of the Eridanus Cloud is bound with over $10^{14} M_{\odot}$ and will ultimately merge.

The first two figures provide information about the group environment. Figure 1 is a histogram of all known velocities within 10,000 km s^{−1} in the projected area shown in Figure 2. The histogram reveals that two structures, the Eridanus Cloud and the Southern Wall, dominate the field in the region of interest. There is no known contamination foreground of the Eridanus Cloud and there is a void behind Eridanus that extends to the Southern Wall. The Southern Wall is 2.5 times more distant so its members are about 2 mag fainter than the equivalent galaxies in Eridanus.

The two panels of Fig. 2 show the distribution of galaxies with known velocities in the Eridanus Cloud and the near-background. The 51–4 group containing NGC 1395 is seen to be nearby but distinct. The NGC 1407 Group is contiguous with the other components of the Eridanus Cloud but there is no suggestion of confusion. Overwhelmingly, candidates within the survey region are early types but most galaxies outside a few discrete knots in Eridanus are late morphological types, very few of which are projected into the survey region.

We do, however, note an unfortunate instance of projection. Three S0 galaxies (NGC 1394 the brightest) in a knot within the Southern Wall lie near the middle of the CFHT survey region. These galaxies are clearly distinguished as background by their velocities, and are not part of the Eridanus Cloud described in the previous paragraph. In the current study, we must give consideration to the possibility that low-surface-brightness companions to these systems

could enter our list of NGC 1407 Group candidates. More distant galaxies are expected to be excluded from our candidate list by the procedures described in section 4.

2.2 X-ray properties

The X-ray-emitting medium in clusters of galaxies is an important tracer of the overall matter distribution. Unfortunately, in groups of galaxies the surface brightness is so low relative to the X-ray background that the emission can rarely be detected beyond a few tenths of a virial radius. The NGC 1407 galaxy was observed by the Einstein (Dressler & Wilson 1985), ROSAT (Davis & White 1996), ASCA (Buote & Fabian 1998), and Chandra (Zhang & Xu 2004) X-ray telescopes. The Chandra observation, which has the best spatial resolution, shows a diffuse X-ray-emitting medium with temperature 0.7 keV and metal abundance about 0.4 solar, a weak central AGN and 40 X-ray point sources, most of which are X-ray binaries. The X-ray luminosity of the diffuse component is 4×10^{40} erg s^{−1} in the 0.3–10 keV band. The NGC 1407 Group is then underluminous by an order of magnitude given the expected value from the X-ray luminosity-temperature and luminosity-velocity dispersion relations (Mahdavi & Geller 2001, Osmond & Ponman 2004).

Because the system is so nearby, the ASCA and Chandra observations of NGC 1407 include little of the group-scale emission outside the central galaxy. The wider field of the ROSAT PSPC detector was able to capture some of this group-scale emission with a resolution of $\approx 15''$ (see Figure 3). Osmond & Ponman (2004) use a β -model to determine a total X-ray luminosity of $\approx 10^{42}$ erg s^{−1} within 570 kpc, which puts the NGC 1407 group directly on the X-ray luminosity-temperature and luminosity-velocity dispersion relations (rather than making it underluminous, as do the Chandra data). One caveat is that an extrapolated β -model can overestimate the gas density at the largest radii (Markevitch et al. 1998). It seems that the NGC 1407 Group is not an X-ray *overluminous* system of galaxies. This is in contrast to the average fossil group, which is overluminous in the X-ray relative to a non-fossil counterpart of the same mass (Khosroshahi et al. 2004; D’Onghia et al. 2005).

The ROSAT data also show significant X-ray emission associated with NGC 1400 and with the probable member dwarf galaxy LEDA 074845. Fitting a MEKAL thermal plasma model to these peaks, we find that the emission in both the peaks comes from gas with the same temperature and metallicity as the gas around NGC 1407. The resulting 0.1–10 keV X-ray fluxes are $1.5 \pm 0.3 \times 10^{-13}$ ergs s^{−1} cm^{−2} for NGC 1400 and $1.1 \pm 0.4 \times 10^{-13}$ erg s^{−1} cm^{−2} for LEDA 074845. We have submitted an XMM-Newton proposal to further investigate the nature of the puzzling emission near LEDA 074845. To our knowledge this is the second reported detection of X-ray emission from NGC 1400—other reports, e.g. Canizares et al. (1987) and Beuing et al. (1999) have been upper limits but O’Sullivan, Forbes and Ponman (2001) report a detection of this galaxy.

Outside the region shown in Figure 3, the ROSAT All Sky Survey shows a lack of X-ray emission from galaxies associated with the NGC 1407 Group (or any other group). Within 0.9 Mpc (2°) of NGC 1407, there are no galaxies,

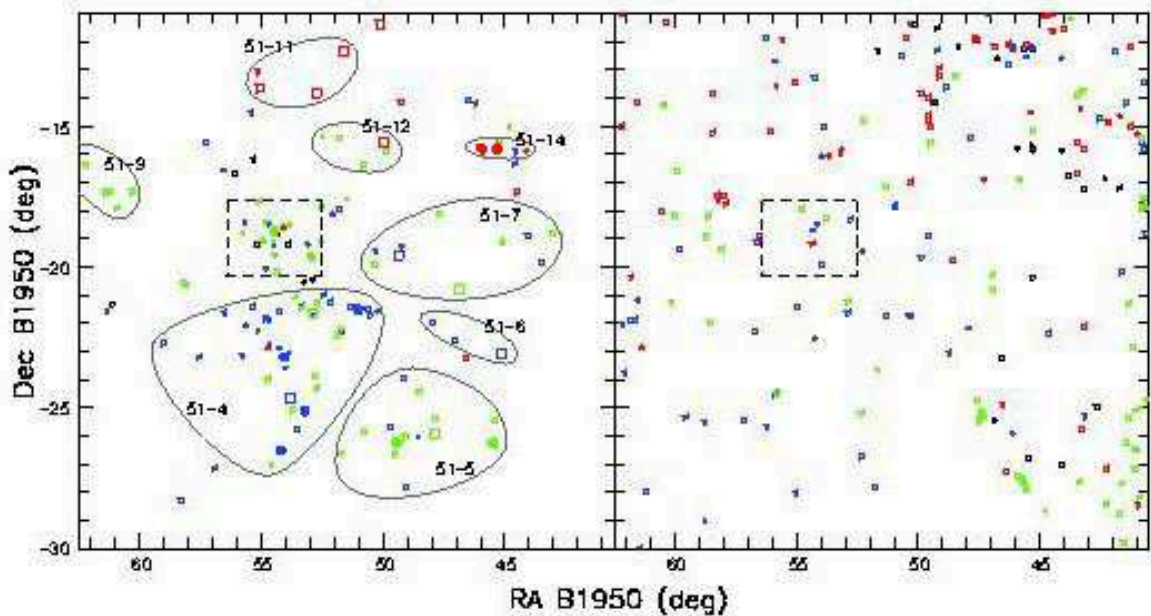


Figure 2. The left panel shows the distribution of galaxies within the velocity range of the Eridanus Cloud ($v < 3000 \text{ km s}^{-1}$). Filled round symbols refer to early-type ($T \leq 1$) galaxies. Open square symbols refer to late-type ($T > 1$) galaxies. More luminous galaxies have larger symbols. Our CFHT survey region around NGC 1407 is indicated by the small rectangle. The irregular enclosed regions indicate the locations of the main groups identified in the Nearby Galaxies Catalog. The 51-4, 51-6, and 51-7 groups have somewhat lower mean velocities than the 51-8 (NGC 1407) group, the 51-5 and 51-9 groups have comparable mean velocities, and the 51-11, 51-12, and 51-14 groups have higher mean velocities. The right panel shows the distribution of galaxies background of the Eridanus Cloud out to $10,000 \text{ km s}^{-1}$.

groups, or clusters with $cz < 20,000 \text{ km s}^{-1}$ that have detectable X-ray emission.

3 OBSERVATIONS AND DATA REDUCTION

3.1 Imaging observations

Observations were made with the Canada-France-Hawaii Telescope (CFHT) 12K CCD camera in queue mode over 6 photometric nights between 8 November and 6 December, 2002. Seeing was 0.6–0.8 arcseconds FWHM. The CFHT 12K camera (Cuillandre et al. 2001) is a mosaic of 12 CCD detectors providing a field of $42' \times 28'$, oriented in this program with the long axis E-W. The observations were made with half-field overlaps so that gaps between CCD chips in any particular exposure were almost entirely filled in and most of the area was observed twice, therefore allowing any non-photometric data to be calibrated. In total, 69×11 minute exposures were taken, all in the Cousins R band, covering 10.05 square degrees. A rectangular area of $220' \times 160'$ was surveyed down to a limiting surface brightness of $1\sigma = 26.5R \text{ mag arcsec}^{-2}$ within an aperture of 2 arcsec FWHM.

TT02 reported deeper observations of the 0.5 sq. deg. core of the NGC 1407 Group obtained with SuprimeCam

on Subaru Telescope. The current observations of 20 times more area were designed to cover the entire virialized region around NGC 1407. In retrospect, we fail slightly to fully cover that region and a small correction for incompleteness will be described.

3.2 Spectroscopy observations

We undertook observations using the blue side of the Low Resolution Imaging Spectrograph (LRIS: Oke et al. 1995) on the Keck I 10m telescope, using a $1''$ slit and a 600 lines in^{-1} grating. Data were acquired on 27 November, 2003. Observations were affected by extensive cirrus and we obtained spectra for only four galaxies. All turned out to be group members. One, N1407-041, also known as APMUK B03381296-184859.2, is revealed to be a second case with a very large blueshift (-932 km s^{-1} with respect to the group mean). Its location in close proximity to NGC 1407 is shown in Figure 3.

4 SAMPLE

Our ultimate intention is to get a listing of group members that is as complete as possible. An unambiguous way to es-

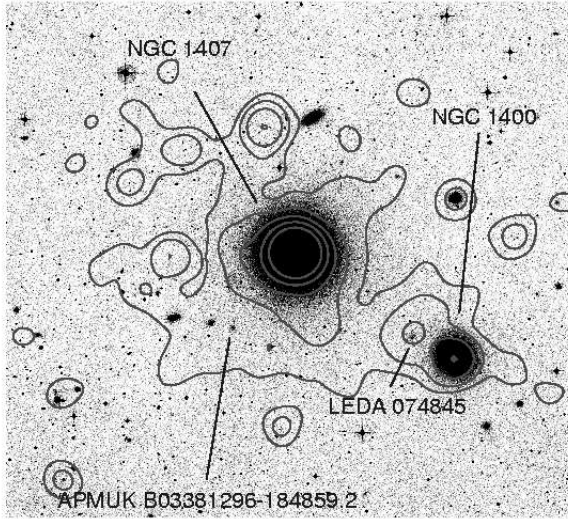


Figure 3. ROSAT X-ray flux contours superposed on an image of the central $35' \times 30'$ region of the NGC 1407 Group. The outermost contours show emission at 2σ significance; each successive contour represents an enhancement in the significance by a factor of 1.5.

Establish membership is to measure a velocity, but velocities can only be obtained for the brighter galaxies. We therefore need to rely on other information to evaluate whether a galaxy lies in the group or not. Dwarf galaxies have low surface brightnesses. If we see a low-surface-brightness galaxy in the direction of the group of a type that we do not see in blank fields, there is a high probability that this galaxy is a low-luminosity member of the group as opposed to a high-luminosity background galaxy. Other information, such as galaxy morphology, can also be useful. For example, if the low-surface-brightness galaxy exhibits spiral structure, it is probably a luminous background galaxy so there is a low probability that it is a dwarf group member. Morphology assessments are subjective but their reliability can be tested. For an extensive discussion of the issues involved with the discovery and confirmation of dwarf galaxies, see Flint et al. (2001).

4.1 Establishing membership using velocity information

A search of the NASA/IPAC Extragalactic Database (NED) reveals 29 galaxies in our survey area have known velocities less than 3000 km s^{-1} . Two additional galaxies have velocities within this limit in the second 6 Degree Field (6dF) data release (Jones et al. 2005). Our Keck observations gave

velocities for four more galaxies, all of which were in the group.

Consequently there are now a total of 35 group members with known velocities, including almost all candidate members brighter than $M_R = -17$. The rms velocity dispersion for these galaxies is $387 \pm 65 \text{ km s}^{-1}$. The projected harmonic mean radius of all group candidates is 446 kpc. These quantities lead to a virial mass of $7.3 \times 10^{13} M_\odot$. From this survey we measure a total group R band luminosity of $2.16 \times 10^{11} L_\odot$. The mass to light ratio is then very large: $M/L_R = 340 M_\odot/L_\odot$.

4.2 Establishing probability of membership using morphology information

We are faced with the problem of establishing membership for galaxies that are too faint to be amenable to spectroscopy. The uncertainties brought about by a purely statistical background subtraction are large and that is why we cannot use this technique. In the 10.05 square degree survey area, we expect about 50 candidate members with $21 > R > 20$, based on knowledge of the field luminosity function (the uncertainty in this function corresponds to about a factor of two in this context). In this same 10.05 square degrees of sky, we expect to find about 20,000 background galaxies in this magnitude interval (see for example Figure 6 of Trentham 1997). The Poisson uncertainty in this number of background galaxies is about 140 but the primary source of uncertainty is large-scale structure along the line of sight. The precise uncertainty depends on exactly where we are looking, but for an area of this size, we would expect a field-to-field variance in the background counts of several times the Poisson uncertainty, about several hundred galaxies. It will therefore not be possible to identify members at any satisfactory level of significance without some other criterion.

Our strategy has been to study such nearby groups that the commonly known dwarf galaxies would all be very well resolved and distinguishable from background galaxies based on surface brightness and morphological criteria. Admittedly, ultracompact dwarfs would escape our attention but so far there is no indication that such high-surface-brightness objects have significant impact on counts at the faint end of the luminosity function. Initially in our program we had no proof that our methodology was valid. However, the analysis of the NGC 5846 group gave us assurance that our selection criteria were working well. We had complete spectroscopic coverage to $M_R = -15$ and sampled coverage to $M_R = -13.3$. We have no proof that our selection criteria are working below this limit but fainter galaxies have even lower mean surface brightnesses and we feel that they separate very well from the background down to $M_R = -12$. Below that limit the dimensions of the candidates get sufficiently small that confusion with the background becomes possible.

Following TT02 and MTT05, we estimate that there is an appreciable probability of membership if the inner (ICP) and outer (OCP) concentration parameters obey the following criteria for bright ($R < 20$) galaxies:

$$\text{ICP} = R(4.4 \text{ arcsec}) - R(2.2 \text{ arcsec}) < 0.7 \quad (1)$$

and

$$\text{OCP} = R(12 \text{ arcsec}) - R(6 \text{ arcsec}) < 0.4. \quad (2)$$

For faint ($R > 20$) galaxies we think that there is an appreciable probability of membership if the galaxy consists of more than three seeing disks with surface brightness $\mu_R < 24.5 \text{ mag arcsec}^{-2}$. These criteria follow from the properties of nearby low-luminosity galaxies. TT02 show how these selection rules favor inclusion of dwarfs and exclusion of background galaxies. All galaxies that meet the selection criteria were examined by eye. We lowered our assessment of the probability of membership if we could see any spiral structure or if the galaxy was very flat, these being properties normally found among high-luminosity galaxies. For each galaxy, we assigned a rating that describes our assessment of the membership probability (e.g. TT02). The ratings have the following meanings:

- “0”: membership confirmed from optical or HI spectroscopic data;
- “1”: probable member, but no spectroscopic or HI detection in the literature;
- “2”: possibly a member, but conceivably background;
- “3”: plausibly a member;
- “4”: passes ICP/OCP surface brightness test but almost certainly background given the morphology of the galaxy and the properties of the background fields studied at various stages during this project;
- “5”: fails ICP/OCP surface brightness test. The vast majority (several thousand with $R < 25$) of galaxies were rated 5.

The discussion below will point out that the vocabulary ‘possible’ and ‘plausible’ were too conservative. Almost all ‘possible’ candidates turn out to be members and a substantial fraction of ‘plausible’ candidates are members.

The analysis of the NGC 5846 group by MTT05 has strengthened the basis of the qualitative ratings. That group has the fortune to lie in a part of the sky with Sloan Digital Sky Survey (SDSS) spectroscopy, which provides essentially complete velocity information to $M_R \sim -15$. Our own Keck LRIS observations provided scattered velocity information to $M_R \sim -13.4$. As a result we could investigate membership issues with an extensive sample of 85 velocities. The investigation was augmented by a correlation analysis of the sort that will be described for the current data in the next section. The analysis carried out on the NGC 5846 Group is directly relevant to the current situation because the two groups are morphologically similar, they are at almost the same distances, and they have been observed with the same instrument and analyzed with the same procedures.

The conclusions reached in MTT05 are that essentially all targets rated 1 and 2 are true group members and that essentially all targets rated 4 are in the background. Concerning objects rated 3, MTT05 concluded that 70% of those brighter than $M_R = -13.4$ (were they to lie at the group distance) are members, 50% of early-type galaxies fainter than this limit are members, and none of the late-type galaxies fainter than this limit are members. We will review these conclusions in the light of the new NGC 1407 Group observations.

Our recipe for identifying group members fails for high surface brightness objects. The extensive SDSS spectroscopic observations of the NGC 5846 region confirmed membership for a small number of high surface brightness ellip-

ticals in the regime $-20 < M_R < -17$, including a system quite similar to the unusual Local Group member M32. Interestingly, the three most extreme high surface brightness objects in that group are all in close proximity to the dominant elliptical NGC 5846 which suggests they may be tidally truncated. Spectroscopy, therefore, provides a useful complement to our procedures, and a survey to a faint limit around NGC 1407 would probably pick up a few currently unsuspected group members. Compact objects have been identified through spectroscopy in other dense groups (Phillipps et al. 2001) but they have not been found in numbers that impact on the luminosity function.

On occasion we misidentify objects as background galaxies on morphological grounds. An example is the case of N5846-256 = CGCG 021-013 in MTT05. Its velocity places it inside the group, but the object looks like a background giant galaxy because it has a substantial dust lane. Another example is the nucleated dwarf elliptical N1407-044 = LSBG F549-036 in the current sample because this galaxy is so flat that we thought it was a background disk galaxies with a bulge. Galaxies like this are extremely rare but it is possible that a small number of the galaxies we rated “4” are actually members.

It is useful to make a comparison with the more sensitive study of the central part of the NGC 1407 Group reported by TT02, based on Subaru 8m observations. In Figure 4, we show the difference between the magnitudes derived from that survey and from the current study. It is clear from this figure that the Subaru magnitudes are systematically brighter. Both studies measure the magnitude above the sky of each galaxy. The Subaru photometry is deeper so the magnitudes represent total light within a fainter isophote. For both datasets the median sky brightness was $20.6 \text{ mag arcsec}^{-2}$. For the Subaru data the 1σ noise within a 0.202 arcsec^2 square pixel was about $26 \text{ mag arcsec}^{-2}$ but it was $25 \text{ mag arcsec}^{-2}$ within a 0.206 arcsec^2 square pixel for the shallower CFHT data. In principle, we could fit exponential disk profiles to the CFHT images and extrapolate to determine total magnitudes but uncertainties for these extremely low surface brightness galaxies would be large (Tully et al. 1996).

The following few galaxies drew attention with this comparison between the CFHT and Subaru data:

N1407-078 = TT02:15: This compact elliptical was rated 5 in the current data and 3 in the Subaru data, which is surprising since most objects tend to be a bit more diffuse in the shallower CFHT data.

N1407-125: This compact galaxy was rated 5 in the Subaru data, but it looks more diffuse in the less deep CFHT data where it was rated 3.

N1407-147 = TT02:26: Once more, this compact elliptical was rated 5 in the current data and 3 in the Subaru data; this is unusual for the reasons described above. It was right on the edge of the chip in the Subaru data, which might explain why it was a bit fuzzy and was rated 3 there.

N1407-160 = TT02:33: This faint galaxy was rated 5 in the current data and 3 in the Subaru data. It is, however, marginal and at a stretch could be rated 3.

N1407-164: This galaxy was rated 5 in deeper Subaru data but this rating was marginal and a rating of 3 is also acceptable.

N1407-168: Like N1407-125, this compact galaxy was rated

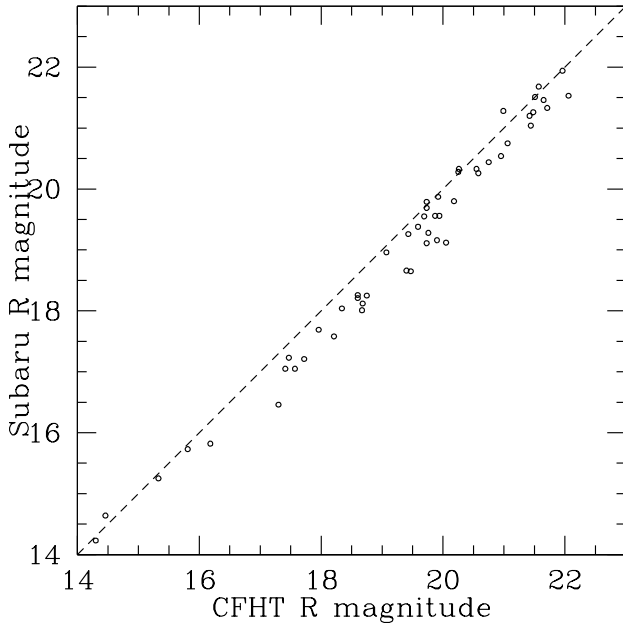


Figure 4. The magnitudes of galaxy in the current survey compared to the magnitudes of the same galaxies measured by TT02 for all galaxies rated 0–3 in both studies.

5 in the Subaru data, but it looks more diffuse in the less deep CFHT data where it was rated 3.

N1407-187: This galaxy fell in a gap between CCD chips in the Subaru data.

N1407-203: This compact galaxy was rated 5 in the Subaru data, but it was rated 3 in the shallower CFHT data.

N1407-239: This galaxy fell in a gap between CCD chips in the Subaru data.

N1407-218 = TT02:50: This galaxy was a rated 5 in the current survey because it looked like a double galaxy. The rating of 3 given by TT02 is marginal.

N1407-241 = TT02:48: This galaxy was marginally detected in the shallower CFHT data. It was indistinguishable from a large number of very faint low-surface-brightness objects in the data, most of which are flat fielding artifacts.

N1407-245 = TT02:53: Once more, this galaxy was marginally detected in the shallower CFHT data but was indistinguishable from the large number of faint low-surface-brightness objects in the data.

N1407-254: This compact galaxy was rated 5 in the Subaru data, but it was rated 3 in the shallower CFHT data.

N1407-261 = TT02:57: Yet again this galaxy was marginally detected in the shallower CFHT data but was indistinguishable from the large number of faint low-surface-brightness objects in the data.

N1407-263: This galaxy resolved into smaller galaxies in the deeper Subaru data and was rated 4.

N1407-265: This very faint galaxy looked like it resolved into two galaxies in the Subaru data and was rated 4.

N1407-267 = TT02:55: This galaxy was undetected in the shallower CFHT data.

N1407-268 = TT02:58: This galaxy was undetected in the shallower CFHT data.

The Subaru observations allowed us to discover fainter candidates but only in a limited area. The objects identified

uniquely with Subaru are included in Table 2 but are flagged and not included in the statistically complete sample.

5 RESULTS

5.1 Spatial correlations

The spatial distribution of candidate members of the NGC 1407 Group are shown in Figure 5. It is apparent that the composition is overwhelmingly early-type: 228 have type Sa or earlier ($T \leq 1$) and 32 are later types ($T \geq 2$).

There is a strong concentration of early-type galaxies toward the center of the group. The combination of the dominance of early types and the central concentration is evidence that the vast majority of the candidates are truly associated with the group. There is a caveat: the projected locations of the three S0 galaxies at 4200 km s^{-1} indicated by the small open triangles are very near the centre of the group. They are known to be background but their neighbors might enter our sample. The possibility is difficult to quantify but this structure is small so we expect that the contamination is also small.

We present two-point correlations for various galaxy subsamples in Figure 6. Following MTT05, the correlations are normalized by comparison with Monte Carlo random catalogs. We do not have a fair sample of the Universe so we give attention only to *relative* variations in correlations.

Very strong correlations are seen in the upper left panel of Fig. 6. The points show the correlation of all types of galaxies that are either known to be members on the basis of velocities or are rated 1 and 2, which we suspect are almost certain to be members. The solid curve gives the correlation if the sample is restricted to only early-type galaxies ($T \leq 1$). These early-type galaxies are slightly more strongly correlated. We do not take the poorer correlation of late types in this sample as evidence that they are not in the group (a half dozen have memberships confirmed by velocities); it would not be surprising if late-types typically live further out from the group center than the early types.

The upper right panel of Fig. 6 shows the correlation of early-type galaxies rated 3 (plausible members) in comparison with the fiducial curve of early-type galaxies with known velocities or rated 0–2. From the weaker correlation one infers that a fraction of those early-type objects rated 3 are not real members. The dotted curve illustrates the correlation found if the fiducial correlation is contaminated with a 20% random population. We conclude that $80 \pm 10\%$ of the early-type galaxies rated 3 are group members.

The correlation of only late-type ($T \geq 2$) galaxies seen in the lower left panel of Fig. 6 is much weaker. However we do not take this as evidence against group membership because a majority of this sub-sample have velocities or are rated 1 or 2. We have not shown the correlation for late-type galaxies rated 3 only because there are just 12 such objects.

The lower right panel of Fig. 6 shows the correlation among only the 34 brightest galaxies. Almost all these galaxies are known to be group members on the basis of velocity measurements. Yet the 2-point correlation is much weaker than for the fiducial sample! The two brightest galaxies, NGC 1407 and NGC 1400, are very close to the group center. On the contrary, the next brightest galaxies, in the range

Table 2. The NGC 1407 Group Sample

ID	Name	Type	Rating	V_h km/s	α (J2000)	δ (J2000)	R_{300}	R	M_R	ID _{TTT}	Rat _{TTT}	R_{TT}
1	NGC 1407	E	0	1779	3 40 11.9	-18 34 49	13.78	9.01	-23.16	1	0	10.23
2	NGC 1400	S0	0	558	3 39 30.8	-18 41 17	13.21	10.37	-21.80	2	0	10.57
3	NGC 1440	S0	0	1534	3 45 02.9	-18 15 57	12.98	10.81	-21.47			
4	NGC 1452	Sa	0	1737	3 45 22.3	-18 38 01	13.51	11.35	-20.90			
5	NGC 1393	S0	0	2185	3 38 38.6	-18 25 40	12.90	11.74	-20.40	3	0	11.45
6	NGC 1383	S0	0	1948	3 37 39.2	-18 20 22	14.09	11.84	-20.36			
7	IC 346	S0	0	2013	3 41 44.7	-18 16 01	14.99	12.24	-19.94			
8	NGC 1359	Sm	0	1966	3 33 47.7	-19 29 31	16.30	12.16	-19.93			
9	ESO 548-G047	S0	0	1606	3 34 43.5	-19 01 44	14.83	12.23	-19.89			
10	ESO 548-G068	S0	0	1693	3 40 19.2	-18 55 53	15.12	12.75	-19.44			
11	IC 343	S0	0	1841	3 40 07.1	-18 26 37	15.16	12.79	-19.39	4	0	12.87
12	ESO 548-G044	Sa	0	1696	3 34 19.2	-19 25 28	15.38	12.86	-19.23			
13	ESO 548-G079	dE,N	0	2016	3 41 56.1	-18 53 43	15.62	13.03	-19.18			
14	ESO 548-G033	S0pec	0	1699	3 32 28.6	-18 56 55	15.32	13.04	-19.05			
15	ESO 548-G064	S0	0	1694	3 40 00.1	-19 25 35	15.19	13.44	-18.75			
16	IC 345	Sa	0	1335	3 41 09.1	-18 18 51	14.30	13.43	-18.75			
17	ESO 548-G076	S0/a	0	1471	3 41 31.8	-19 54 19	16.90	13.48	-18.70			
18	NGC 1390	Sa	0	1207	3 37 52.2	-19 00 30	16.35	13.64	-18.52			
19	ESO 548-G063	Sdm	0	1988	3 39 34.8	-20 00 53	16.95	14.03	-18.12			
20	ESO 548-G082	Sd	0	1716	3 42 43.3	-17 30 26	18.23	14.39	-17.90			
21	LEDA 074868	E	0	1575	3 40 15.9	-19 04 54	16.56	14.32	-17.85			
22	ESO 548-G043	Sd	0	1931	3 34 10.5	-19 33 30	15.64	14.27	-17.81			
23	ESO 548-G002	Sm	0	1111	3 42 57.3	-19 01 12	17.70	14.39	-17.80			
24	ESO 548-G065	Sa	0	1221	3 40 02.7	-19 22 00	17.82	14.40	-17.80			
25	LEDA 074886	E	0	1308	3 40 43.2	-18 38 43	16.29	14.30	-17.79	5	0	14.23
26	APMBGC 549+118-079	Sd	0	1979	3 44 02.5	-18 28 18	17.80	14.45	-17.75			
27	ESO 548-G073	Sdm	0	989	3 41 04.4	-19 05 40	17.50	14.46	-17.74			
28	ESO 549-G007	E	0	1527	3 44 11.5	-19 19 13	17.11	14.43	-17.72			
29	APMBGC 548-110-078	E	0	1595	3 40 52.7	-18 28 40	16.88	14.46	-17.71	6	0	14.64
30	LEDA 135109	E	3		3 43 42.7	-19 49 48	15.74	14.50	-17.66			
31	LEDA 074924	E	2		3 41 59.9	-18 42 47	16.85	14.76	-17.42			
32	APMBGC 548-118-089	E	2		3 41 29.8	-18 15 50	17.23	14.87	-17.32			
33	ESO 548-G072	Sm	0	2034	3 41 00.3	-19 27 19	18.34	15.01	-17.20			
34	LSBG F549-032	dE,N	2		3 42 47.5	-17 34 04	17.99	15.30	-17.00			
35	APMBGC 548-122-018	Epec	0	1913	3 41 49.8	-19 34 53	17.98	15.32	-16.87			
36	LEDA 074838	dE,N	2		3 39 23.1	-18 45 30	17.67	15.33	-16.84	7	1	15.25
37	LSBG F548-012	dE,N	2		3 38 42.1	-18 53 59	18.54	15.52	-16.66			
38	2MASXi J0341186-180206	E	3		3 41 18.6	-18 02 07	17.36	15.76	-16.64			
39	APMUKS B033659.29-185352.7	dE,N	2		3 39 14.5	-18 44 10	17.57	15.81	-16.35	8	2	15.73
40	2MASXi J0341237-183808	E	3		3 41 23.7	-18 38 08	17.76	16.05	-16.12			
41	LSBG F548-006	dE,N	0	698	3 40 33.8	-18 39 03	18.66	16.18	-16.00	9	1	15.82
42	LSBG F548-016	dE,N	2		3 35 10.7	-18 55 51	18.59	16.19	-15.93			
43	LSBG F549-023	dE,N	2		3 44 10.7	-17 49 59	18.69	16.40	-15.90			
44	LSBG F549-036	dE,N	0	2101	3 41 46.6	-17 44 22	18.44	16.45	-15.75			
45	2MASX J03425744-1900411	E	2		3 42 57.4	-19 00 41	17.32	16.47	-15.73			
46	N1400GR:[FS90] 079	dE	3		3 41 10.1	-17 38 13	18.79	16.60	-15.67			
47	LSBG F549-038	dE,N	0	1893	3 40 49.7	-18 50 50	18.59	16.70	-15.52			
48	LSBG F548-026	dE,N	0	1492	3 39 33.9	-19 15 58	18.49	16.67	-15.51			
49	N1400GR:[FS90] 067	dE,N	3		3 40 47.4	-18 37 11	18.73	16.71	-15.46			
50	APMUKS B033801.24-191219.0	dI	3		3 40 16.0	-19 02 41	18.75	16.85	-15.33			
51	APMUKS B033224.45-192557.3	dE	2		3 34 39.4	-19 15 58	19.18	16.78	-15.31			
52	LSBG F548-003	dI	3		3 42 54.8	-17 33 23	18.92	17.11	-15.20			
53	LSBG F548-032	dE	2		3 33 11.5	-19 19 02	18.90	17.10	-14.99			
54	LSBG F549-021	dE,N	3		3 45 09.4	-17 55 08	19.11	17.27	-14.99			
55	LEDA 074762	dE	1		3 36 05.9	-17 52 36	20.12	17.33	-14.88			

ID	Name	Type	Rating	V_h km/s	α (J2000)	δ (J2000)	R_{300}	R	M_R	ID _{TT}	Rat _{TT}	R_{TT}
56	LEDA 074845	dI	1		3 39 42.0	-18 40 03	20.51	17.30	-14.87	10	1	16.46
57	LEDA 074830	dE,N	1		3 39 04.5	-18 31 56	19.29	17.41	-14.75	12	2	17.05
58	LSBG F548-011	dE,N	2		3 39 04.6	-18 21 36	19.17	17.47	-14.70	14	3	17.23
59		dE	2		3 37 51.3	-18 38 45	19.41	17.57	-14.63			
60	APMUKS B033247.49-182749.0	dE	3		3 35 03.4	-18 17 52	19.34	17.56	-14.63			
61	LSBG F549-037	dE	3		3 40 54.8	-17 31 30	19.88	17.64	-14.63			
62	LEDA 074847	dE,N	1		3 39 45.4	-18 30 16	20.13	17.57	-14.60	11	1	17.05
63		dI	3		3 34 32.8	-19 01 03	19.07	17.54	-14.58			
64	APMUKS B033659.86-195850.8	dE	3		3 39 13.8	-19 49 08	19.73	17.63	-14.54			
65	N1400GR:[FS90] 058	dE,N	1		3 40 28.2	-18 39 22	19.37	17.72	-14.46	13	1	17.21
66	APMUKS B033423.76-194449.4	dI	1		3 36 38.2	-19 34 57	19.53	17.76	-14.34			
67	LEDA 074891	dE,N	1		3 40 50.0	-18 05 29	20.05	17.90	-14.29			
68	APMUKS B034054.06-195241.1	dI/E	1		3 43 08.0	-19 43 13	21.07	17.92	-14.27			
69	LSBG F548-005	dE,N	3		3 42 13.2	-18 56 51	19.57	17.96	-14.24			
70		dE/N	1		3 40 00.9	-18 48 14	19.70	17.96	-14.21	16	1	17.69
71	APMUKS B033739.33-185912.5	dE	3		3 39 54.4	-18 49 33	19.52	18.04	-14.13			
72	N1400GR:[FS90] 012	dE	1		3 37 52.2	-18 55 27	20.48	18.05	-14.12			
73	APMUKS B033150.50-193739.6	dE	3		3 34 05.0	-19 27 43	19.96	18.03	-14.06			
74	LSBG F549-025	dE	3		3 43 54.4	-18 30 07	19.89	18.21	-13.99			
75		dE	1		3 38 26.2	-18 00 07	20.76	18.28	-13.94			
76	N1400GR:[FS90] 059	dE,N	1		3 40 28.8	-18 58 17	20.68	18.29	-13.89			
77	APMUKS B033150.50-193739.6	dE	3		3 34 05.2	-19 27 37	20.33	18.22	-13.87			
78	APMUKS B033912.64-183429.9	dE,N	3*		3 41 27.7	-18 24 57	19.66	18.21	-13.87	15	3	17.58
79	N1400GR:[FS90] 032	dE,N	1		3 39 09.2	-18 26 44	20.31	18.31	-13.85			
80	N1400GR:[FS90] 033	dE,N	2		3 39 09.7	-18 37 28	19.90	18.34	-13.82	18	2	18.04
81	APMUKS B033329.47-184051.6	dE	2		3 35 45.1	-18 30 58	19.96	18.34	-13.80			
82		dE,N	3		3 41 54.0	-17 38 50	20.23	18.53	-13.76			
83	LSBG F549-018	dI	3		3 45 48.4	-18 50 36	20.41	18.48	-13.75			
84	LEDA 074784	dE	3		3 37 03.7	-18 58 18	19.66	18.43	-13.71			
85		dI	3		3 39 19.3	-19 19 40	21.19	18.54	-13.62			
86		VLSB	1		3 38 49.1	-18 42 13	21.48	18.60	-13.58	22	1	18.26
87	APMUKS B033057.83-175450.4	dI	3		3 33 14.3	-17 44 50	20.46	18.63	-13.58			
88	LEDA 074854	dE,N	2		3 39 53.3	-18 37 17	19.93	18.60	-13.57	20	2	18.21
89	APMUKS B033402.22-194037.3	dE,N	1		3 36 16.8	-19 30 43	19.86	18.53	-13.57			
90	APMUKS B034324.69-182212.5	dE,N	1		3 45 40.1	-18 12 55	20.90	18.72	-13.56			
91	APMUKS B034020.33-195428.2	dE	3		3 42 34.2	-19 44 58	20.23	18.63	-13.54			
92	N1400GR:[FS90] 044	dE,N	2		3 39 48.8	-18 53 20	20.23	18.65	-13.52			
93	LEDA 074814	dE	1		3 38 28.3	-18 00 05	20.65	18.71	-13.51			
94	LEDA 074804	dE,N	2		3 37 58.8	-18 42 42	20.02	18.70	-13.50			
95		dE	3		3 36 05.7	-18 23 02	20.03	18.67	-13.50			
96	LEDA 074857	dE,N	1		3 39 59.5	-18 29 20	20.59	18.68	-13.50	19	1	18.12
97	N1400GR:[FS90] 032	dE,N	1		3 39 09.1	-18 26 42	20.19	18.67	-13.49	17	2	18.01
98		dE,N	1		3 40 59.0	-17 43 04	22.25	18.75	-13.49			
99	N1400GR:[FS90] 102	dE	1		3 43 25.2	-17 51 16	20.83	18.86	-13.47			
100	N1400GR:[FS90] 045	dE	2		3 39 51.3	-18 27 59	20.31	18.75	-13.43	21	1	18.25
101	APMUKS B034300.92-191231.4	dE,N	2		3 45 15.4	-19 03 11	21.38	18.81	-13.41			
102		dE	1		3 40 07.4	-17 58 49	21.09	18.79	-13.40			
103	APMUKS B033515.30-200435.9	dE	3		3 37 29.4	-19 54 49	20.28	18.71	-13.39			
104		dE	1		3 39 32.4	-19 25 16	21.01	18.80	-13.37			
105		VLSB	1		3 37 28.7	-19 11 15	22.25	18.77	-13.37			
106	APMUKS B033220.92-201714.6	dE/I	2		3 34 34.9	-20 07 16	20.79	18.74	-13.33			
107		dE/I	2		3 46 50.0	-19 48 28	21.30	18.96	-13.32			
108		dI	3		3 39 27.4	-17 30 35	20.38	18.92	-13.32			
109		dE	1		3 35 40.9	-18 43 41	20.87	18.85	-13.28			
110	LEDA 074765	dE	3		3 36 07.2	-18 22 43	20.00	18.92	-13.25			

ID	Name	Type	Rating	V_h km/s	α (J2000)	δ (J2000)	R_{300}	R	M_R	ID _{TT}	Rat _{TT}	R_{TT}
111		dE	2		3 39 33.0	-18 07 16	20.65	18.97	-13.23			
112	APMUKS B033605.04-182859.2	dI	3		3 38 20.8	-18 19 15	19.98	19.00	-13.17			
113	LEDA 074878	dE,N	1		3 40 30.7	-17 46 00	20.33	19.06	-13.16			
114	N1400GR:[FS90] 031	dE,N	3		3 39 07.0	-18 59 16	20.19	19.04	-13.13			
115		dE	1		3 39 51.0	-18 32 23	21.75	19.07	-13.10	25	1	18.96
116		dE/I	2		3 35 24.0	-19 41 40	20.80	19.03	-13.06			
117		dE	1		3 37 39.0	-19 09 50	21.05	19.11	-13.04			
118	APMUKS B034533.53-193604.0	dE/I	2		3 47 47.8	-19 26 54	21.12	19.22	-13.00			
119		dE,N	2		3 35 26.0	-19 41 27	20.81	19.10	-12.99			
120		dE,N	1		3 40 28.1	-18 19 31	21.17	19.19	-12.98			
121	N1400GR:[FS90] 007	dE	3		3 37 17.0	-18 10 31	20.39	19.23	-12.94			
122		dE	1		3 35 09.9	-18 38 33	21.71	19.23	-12.93			
123		dE	2		3 35 25.2	-18 41 55	20.56	19.23	-12.92			
124		dE	1		3 40 55.8	-18 49 15	21.32	19.35	-12.87			
125	N1400GR:[FS90] 046	dE,N	3		3 39 52.6	-18 46 51	20.11	19.32	-12.85		4	
126		dE	1		3 40 33.7	-19 07 07	22.41	19.35	-12.83			
127		dE/I	2		3 36 43.0	-18 02 11	20.53	19.37	-12.81			
128		dE,N	1		3 38 11.5	-18 22 56	21.10	19.40	-12.78	24	1	18.66
129		dE	2		3 44 50.1	-19 18 31	20.87	19.40	-12.78			
130		dE	2		3 42 02.3	-18 26 37	21.20	19.43	-12.76	29	2	19.26
131		dE	3		3 45 04.4	-18 36 18	20.63	19.50	-12.74			
132		dE,N	1		3 40 02.6	-18 22 36	21.15	19.45	-12.73			
133		dE	3		3 41 44.3	-19 11 35	20.46	19.46	-12.73			
134		dE,N	1		3 40 02.6	-18 22 36	20.88	19.47	-12.71	23	1	18.65
135		dE	3		3 35 42.2	-18 03 19	20.67	19.51	-12.68			
136	N1400GR:[FS90] 014	dE	1		3 37 54.58	-19 00 18	20.26	19.50	-12.66			
137		dE	2		3 35 55.2	-18 41 29	20.54	19.48	-12.65			
138		VLSB	2		3 39 46.1	-18 13 06	23.41	19.55	-12.64			
139		dI/V	2		3 41 31.1	-18 52 35	23.31	19.61	-12.61			
140	N1400GR:[FS90] 063	dE,N	2		3 40 44.0	-18 44 40	20.76	19.59	-12.61	31	2	19.38
141		dE,N	3		3 39 00.0	-18 06 30	20.78	19.62	-12.59			
142		dE	3		3 37 03.2	-18 48 58	20.87	19.60	-12.54			
143	N1400GR:[FS90] 095	dE	2		3 42 31.6	-18 32 29	21.38	19.66	-12.51			
144		dE	2		3 35 38.4	-18 54 52	20.46	19.64	-12.50			
145		dI	2		3 39 50.8	-18 22 51	21.43	19.69	-12.50	32	3	19.55
146		dE	2		3 42 06.1	-19 35 55	21.12	19.71	-12.48			
147		dE	3*		3 39 55.1	-18 21 22	20.71	19.73	-12.46	26	3	19.11
148	N1400GR:[FS90] 073	dE,N	1		3 40 56.6	-18 39 22	21.50	19.73	-12.45	36	2	19.79
149		dE,N	1		3 38 28.5	-18 46 22	21.29	19.76	-12.44	30	2	19.28
150		dE,N	2		3 39 42.0	-18 42 58	21.42	19.73	-12.43	35	2	19.69
151	N1400GR:[FS90] 115	dE,N	1		3 45 23.3	-18 07 24	20.95	19.82	-12.43			
152		dE	2		3 36 07.5	-18 11 04	20.79	19.76	-12.43			
153		dE	2		3 36 03.1	-18 48 59	20.97	19.71	-12.42			
154		dE/I	3		3 35 15.9	-19 18 26	20.98	19.69	-12.41			
155		dE	3		3 39 25.9	-18 52 05	20.70	19.77	-12.40			
156		dE	2		3 41 42.5	-18 59 11	21.36	19.84	-12.36			
157		dE	1		3 37 38.6	-18 21 37	20.89	19.83	-12.36			
158		dE	2		3 37 35.0	-18 33 27	20.99	19.84	-12.35			
159		dE/I	2		3 39 04.0	-18 19 22	21.47	19.84	-12.34			
160		dE	3*		3 41 27.8	-18 42 28	20.95	19.87	-12.32	33	3	19.56
161	N1400GR:[FS90] 062	dE,N	1		3 40 37.6	-18 32 45	21.09	19.90	-12.27	28	2	19.16
162		dE	2		3 33 19.9	-18 41 09	21.53	19.84	-12.26			
163		dE	2		3 42 17.8	-18 47 19	21.32	19.94	-12.26			
164		dE,N	3		3 39 58.1	-18 37 36	21.69	19.92	-12.25		4	
165	N1400GR:[FS90] 080	dE	3		3 41 14.2	-18 38 26	20.87	19.92	-12.24	38	2	19.87

ID	Name	Type	Rating	V_h km/s	α (J2000)	δ (J2000)	R_{300}	R	M_R	ID_{TT}	Rat_{TT}	R_{TT}
166	N1400GR:[FS90] 070	dE	1		3 40 51.5	-18 29 44	21.42	19.94	-12.22	34	1	19.56
167		dE,N	1		3 39 13.9	-18 53 43	21.43	19.96	-12.22			
168		dE	3		3 38 11.5	-18 24 20	20.68	20.04	-12.15		4	
169		dE	3		3 38 10.6	-18 18 58	21.72	20.03	-12.14			
170		dE	2		3 35 31.5	-19 50 06	21.45	19.97	-12.12			
171		dI	2		3 33 41.2	-19 00 45	21.34	19.99	-12.11			
172		dE	2		3 35 06.4	-17 38 08	21.31	20.10	-12.10			
173		dE/I	1		3 46 02.8	-18 19 18	22.41	20.21	-12.06			
174		dE	3		3 39 02.6	-18 00 30	21.18	20.16	-12.06			
175		dE,N	1		3 38 52.0	-18 26 00	21.19	20.05	-12.03	27	1	19.12
176		dE,N	2		3 39 11.4	-18 55 32	21.44	20.18	-11.99			
177		dE,N	2		3 39 42.4	-19 38 28	21.31	20.19	-11.98			
178		dE,N	2		3 39 22.3	-18 31 59	21.53	20.18	-11.98	37	1	19.80
179		dE	3		3 40 26.4	-20 06 50	21.17	20.03	-11.96			
180		dE	2		3 38 10.4	-18 34 22	21.37	20.25	-11.94	39	2	20.28
181		dE,N	2		3 43 01.6	-18 37 35	21.39	20.23	-11.94			
182		dE/I	2		3 47 31.8	-18 50 34	21.38	20.30	-11.93			
183		dE,N	2		3 38 38.8	-18 42 16	21.01	20.26	-11.93	41	3	20.33
184		dE/I	2		3 38 26.9	-18 56 26	21.23	20.26	-11.92			
185		dE,N	2		3 40 31.2	-17 54 05	21.63	20.29	-11.91			
186		dI	2		3 42 32.4	-19 21 56	22.08	20.26	-11.90			
187		dE,N	3		3 38 33.1	-18 44 08	21.32	20.30	-11.90			
188		dE/I	1		3 34 17.3	-19 04 30	22.54	20.23	-11.88			
189		dE	2		3 40 31.5	-18 15 05	21.76	20.30	-11.87			
190		dE	2		3 37 29.8	-18 32 23	21.42	20.32	-11.86			
191		dE,N	3		3 41 03.3	-18 04 18	20.97	20.37	-11.83			
192		dE/I	1		3 40 30.5	-17 34 08	22.16	20.49	-11.80			
193		dE	3		3 38 46.2	-19 53 15	21.72	20.34	-11.79			
194		dE,N	3		3 40 37.5	-18 56 50	21.19	20.43	-11.76			
195		dE	3		3 38 06.3	-19 28 58	21.46	20.39	-11.76			
196		dE/I	2		3 42 27.2	-18 46 20	21.94	20.46	-11.73			
197		dI	3		3 39 49.3	-18 20 12	21.34	20.51	-11.68			
198		dE/I	1		3 40 41.8	-18 26 11	22.71	20.55	-11.62	42	1	20.33
199		dI/E	3		3 43 26.6	-19 46 26	21.77	20.56	-11.61			
200		dE	3		3 43 30.6	-18 31 39	22.05	20.60	-11.59			
201		dE,N	2		3 39 42.3	-18 39 20	21.32	20.58	-11.58	40	3	20.26
202		dE,N	3		3 41 19.3	-18 16 58	21.47	20.62	-11.57			
203		dE,N	3		3 40 45.1	-18 48 14	21.36	20.69	-11.52		4	
204		dE/I	3		3 42 46.7	-17 49 07	22.84	20.80	-11.51			
205		dE	3		3 42 04.6	-17 31 55	22.61	20.79	-11.49			
206		dE/I	3		3 41 12.5	-18 46 10	22.87	20.73	-11.48			
207		dE/I	3		3 40 00.0	-18 23 46	21.44	20.75	-11.44	43	3	20.44
208		dE	3		3 41 09.9	-17 45 06	21.45	20.82	-11.41			
209		dE	1		3 37 51.1	-18 21 41	22.08	20.81	-11.38			
210		dE,N	3		3 40 45.2	-18 48 12	21.28	20.84	-11.37			
211		dE	1		3 41 53.6	-18 26 32	23.63	20.82	-11.37			
212		dE	2		3 39 29.7	-18 12 52	21.66	20.84	-11.36			
213		dI	3		3 43 12.2	-19 27 24	22.74	20.82	-11.32			
214		dE,N	3		3 41 33.2	-17 56 32	21.89	20.89	-11.31			
215		dE/I	2		3 34 11.8	-18 14 21	22.53	20.85	-11.31			
216		dE	3		3 41 23.1	-18 44 21	23.45	20.91	-11.30			
217		dE	3		3 39 20.9	-18 15 29	21.80	20.92	-11.27			
218		dI	3*		3 39 36.3	-18 34 45	21.62	20.93	-11.17	50	3	20.99
219		dE/I	2		3 40 11.1	-18 19 31	21.62	21.01	-11.17			
220		dE/I	3		3 47 50.5	-19 58 01	22.13	21.09	-11.15			

ID	Name	Type	Rating	V_h km/s	α (J2000)	δ (J2000)	R_{300}	R	M_R	ID _{TT}	Rat _{TT}	R_{TT}
221		dE,N	1		3 38 59.5	-18 27 27	22.76	20.95	-11.14	45	1	20.54
222		dE	2		3 37 08.4	-18 10 10	22.18	21.04	-11.13			
223		dE	3		3 38 05.5	-18 50 25	22.48	21.07	-11.13			
224		dE	2		3 40 25.5	-18 37 57	22.56	21.06	-11.12	46	2	20.75
225		dE	2		3 39 06.1	-18 19 45	21.98	21.08	-11.10			
226		dE,N	2		3 37 24.9	-18 41 37	21.93	21.09	-11.09			
227		dE,N	2		3 39 53.1	-17 57 32	22.45	21.12	-11.07			
228		dE/I	2		3 37 51.3	-18 21 39	22.07	21.12	-11.07			
229		dE/I	3		3 45 41.2	-18 29 09	22.27	21.22	-11.06			
230		dE	2		3 44 26.2	-17 54 38	21.75	21.25	-11.04			
231		dE/I	3		3 43 39.1	-18 57 05	22.40	21.22	-11.01			
232		dE/I	3		3 47 00.5	-17 47 32	22.47	21.21	-11.01			
233		dE/I	3		3 35 08.3	-18 00 18	22.00	21.23	-10.97			
234		dE,N	3		3 41 04.4	-17 52 32	22.86	21.25	-10.95			
235		dE	3		3 35 18.5	-17 48 36	21.51	21.32	-10.89			
236		dE,N	2		3 38 04.0	-18 53 43	22.28	21.33	-10.85			
237		dE/I	3		3 40 52.3	-19 14 14	22.18	21.35	-10.85			
238		dE/I	2		3 40 37.9	-18 16 13	22.04	21.34	-10.83			
239		dE/I	3		3 40 22.7	-18 37 02	22.51	21.38	-10.80			
240		dE,N	3		3 34 16.7	-18 32 32	21.38	21.35	-10.78			
241		dI	3*		3 40 16.1	-18 41 35	23.09	21.42	-10.76	48	2	21.20
242		dE/I	3		3 40 06.6	-18 24 42	21.85	21.44	-10.74	47	3	21.04
243		dI	2		3 41 53.0	-18 14 49	22.74	21.45	-10.73			
244		dE/I	3		3 35 23.3	-19 46 44	21.96	21.40	-10.69			
245		dI	3*		3 40 44.0	-18 44 40	22.25	21.51	-10.69	53	2	21.51
246		dI	2		3 40 56.6	-18 30 40	22.37	21.48	-10.68	49	2	21.26
247		dI	3		3 42 30.5	-19 52 18	22.83	21.53	-10.64			
248		dE	3		3 40 50.7	-17 45 42	21.70	21.60	-10.63			
249		dE/I	3		3 40 27.3	-18 42 30	21.86	21.57	-10.62	56	3	21.68
250		dE/I	3		3 41 03.3	-17 50 33	22.47	21.64	-10.57			
251		dE	3		3 42 02.2	-18 18 20	22.27	21.61	-10.56			
252		dE/I	2		3 40 48.8	-18 30 27	22.79	21.65	-10.51	52	2	21.46
253		dE	2		3 38 12.7	-18 13 43	22.35	21.67	-10.50			
254		dE	2		3 39 23.3	-18 33 16	22.41	21.70	-10.46		4	
255		dI	3		3 39 57.3	-18 38 43	21.85	21.71	-10.46	51	3	21.33
256		dE/I	3		3 33 35.9	-18 27 34	22.62	21.69	-10.42			
257		dE/I	2		3 41 09.1	-19 05 50	22.67	21.82	-10.38			
258		dE/I	3		3 36 24.3	-18 44 41	22.86	21.76	-10.37			
259		dE/I	3		3 42 24.0	-18 54 19	22.46	21.90	-10.30			
260		dE,N	3		3 40 49.0	-18 48 35	22.27	21.93	-10.28			
261		dI	3*		3 39 11.3	-18 34 11	22.69	21.96	-10.20	57	3	21.94
262		dE	3		3 41 27.1	-18 46 09	22.47	22.06	-10.15	54	3	21.53
263		dE/I	3		3 39 50.4	-18 35 59	22.39	22.06	-10.11		4	
264		dE	3		3 41 08.7	-18 46 22	23.39	22.25	-9.96			
265		dE/I	3		3 40 32.1	-18 44 43	22.45	22.25	-9.95		4	
266		dE/I	2		3 41 06.0	-19 05 37	22.71	22.33	-9.89			
267		dI			3 39 53.5	-18 27 54				55	2	21.58
268		dI			3 38 25.2	-18 33 51				58	2	22.00

$0.04 - 1L^*$ are relatively dispersed compared with the fiducial population numerically dominated by early-type dwarfs.

We draw the following conclusions about our subjective ratings from the spatial correlations. There is no reliable information that contradicts the conclusions of MTT05 drawn from the NGC 5846 Group analysis that systems rated 1 or 2 are very likely to be group members and that systems rated 4 are very likely to be background. We find that the background contamination within the sample of early-type objects rated 3 is a bit smaller in the NGC 1407 Group ($\sim 20\%$) than in the NGC 5846 Group (30 – 50% depend-

ing on luminosity). The late-type dwarfs are more weakly correlated but we cannot decide whether that is due to contamination or a consequence of an intrinsically weaker correlation (as could arise if late types arrived more recently in the group).

Our sample from the CFHT survey amounts to 260 galaxies (9 additional galaxies listed in Table 2 are from the deeper but limited Subaru survey and are not considered part of the statistical sample). About 34 additional candidates would be expected to be found if the CFHT survey were extended to fill the 2° circle corresponding to

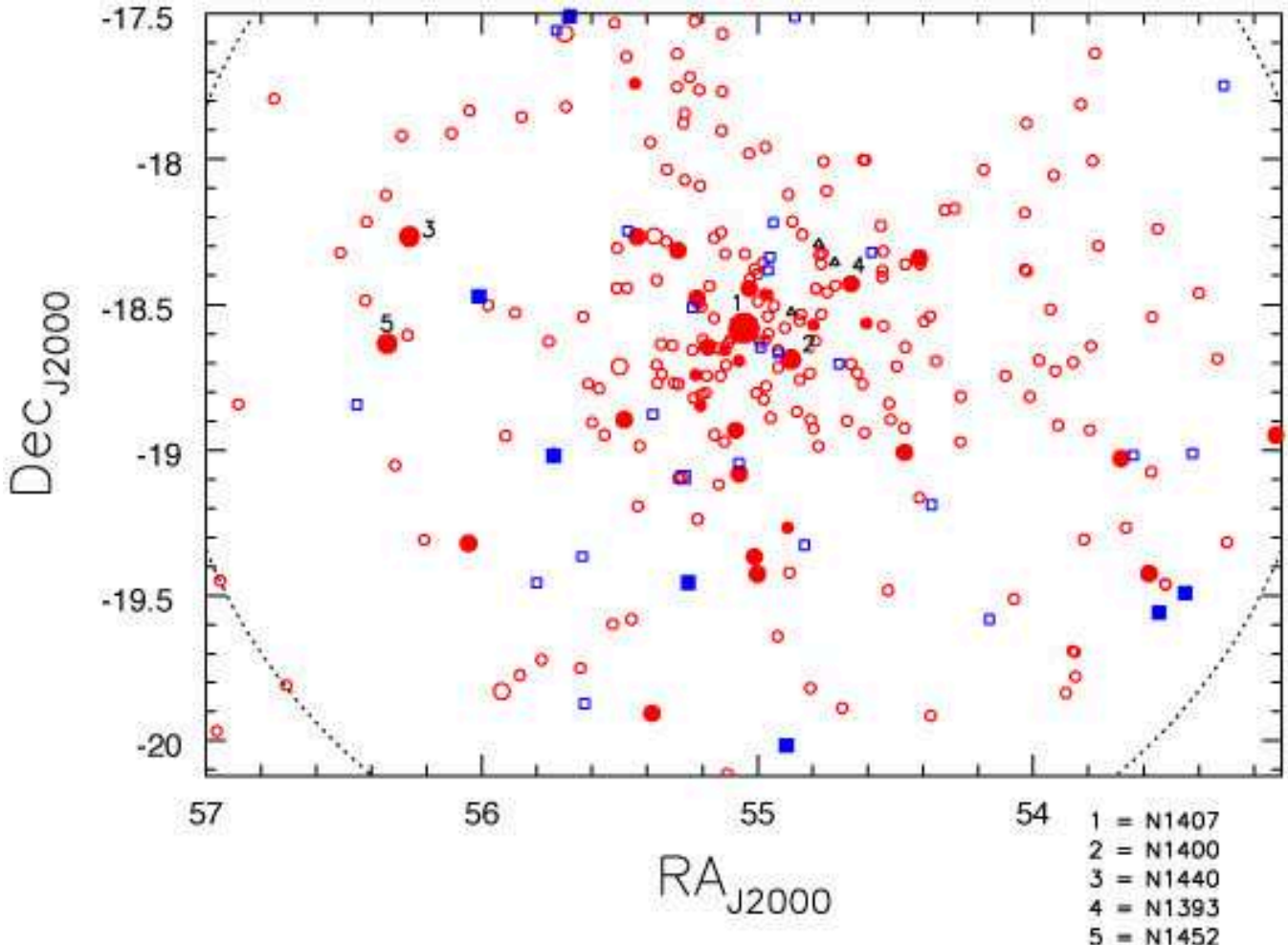


Figure 5. Positions of candidate NGC 1407 Group members. Circles represent early-type galaxies and boxes represent late-type galaxies. Galaxies with filled symbols have their membership confirmed with a velocity. Large symbols represent galaxies with $M_R < -17$. The five most luminous galaxies are identified. Three galaxies in the background within the Southern Wall are indicated by small triangles. The outer dotted circle has a radius of 2 degrees.

the second turnaround radius described later in this section. Roughly 47 of the ensemble of candidates are expected on statistical grounds to be background contaminants. In summary we expect the NGC 1407 to contain $\sim 250 \pm 20$ galaxies to the limit of our survey.

5.2 The distinct radial distributions of dwarfs and giants

The spatial correlation differences brought to light in Fig. 6 are shown in another way in Fig. 7. Here we show the cumulative radial distributions of dwarf ellipticals ($M_R > -17$) and of all bright group members ($M_R \leq -17$). The luminous galaxies are less concentrated toward the center of the group than the dwarf galaxies; these two populations have 50 percentile radii of $0.79^\circ = 350$ kpc and $0.55^\circ = 240$ kpc respectively. Miles et al. (2004) draw attention to an apparent dip in the luminosity function in X-ray dim groups. They ascribe this feature to dynamical evolution, with intermediate-mass systems merging with the central massive system on shorter timescales than lower-mass systems. A similar pro-

cess may be operating here and may generate the observed phenomenon. The radial scale of the effect manifested in Fig. 7 is $\sim 1^\circ$, roughly half the virial radius. Jones et al. (2003) point out that orbital decay by dynamical friction will cause an L^* galaxy to fall from this radius to the center of an NGC 1407-like group in a Hubble time.

5.3 The second turnaround radius

In the case of the NGC 5846 Group, MTT05 claimed to identify a drop in the radial density distribution and the radial velocity distribution at a radius of 840 kpc which was identified as the caustic of second turnaround (Bertschinger 1985). The NGC 5846 analysis benefited from the availability of a complete sample of velocities down to $M_R \sim -15$ across an extent much larger than the group from the Sloan Digital Sky Survey. There were three times more velocities available within that group and the domain beyond the group could be characterized.

With collisionless spherical collapse, the surface of second turnaround today corresponds to the same density level

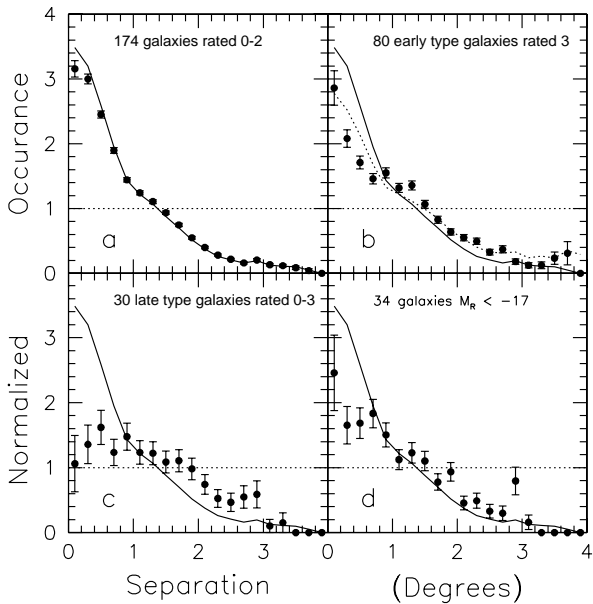


Figure 6. Two-point correlation functions. Pairwise separations are compared against Monte Carlo random distributions for several subsets of galaxies in the CFHT survey region around NGC 1407. In panel *a*, the points with error bars represents the correlation found among the 172 galaxies either with velocities that identify them as group members or rated 1 and 2, hence almost certainly group members. The solid line demonstrates the correlation with the 154 galaxies typed Sa or earlier and with a velocity or rated 1 and 2. This highly correlated sample provides a reference which is carried over to all the panels. In panel *b* one sees the correlation among 80 early types rated 3. The slightly weaker correlation can be matched by mixing the reference correlation with a 20% addition of randomly distributed objects. Panels *c* and *d* show the weaker correlations that are found among 30 galaxies typed later than Sa and among 34 galaxies brighter than $M_R = -17$, respectively. In the case of the brighter galaxies, most of the systems have measured velocities that confirm membership so the weaker correlation indicates this population is more dispersed in the group. The weaker correlation among late types may at least in part have a similar origin.

for all collapsed objects. Comparing the second turnaround radii $r_{2t,i}$ of two groups or clusters of mass M_i , $i = 1, 2$:

$$M_1/M_2 = (r_{2t,1}/r_{2t,2})^3. \quad (3)$$

Using the NGC 5846 calibration, then r_{2t} for a group of mass M_{12} in mass units of $10^{12} M_\odot$ is

$$r_{2t} = 0.193(M_{12})^{1/3} \text{ Mpc.} \quad (4)$$

Using the virial approximation, with $M \propto \sigma_v^2 r_{2t}$,

$$r_{2t} = \sigma_v/390 \text{ Mpc.} \quad (5)$$

Equations 4 and 5 give alternate values for $r_{2t}^{NGC1407}$ of 810 kpc (1.84°) and 990 kpc (2.27°). An approximate value for the second turnaround radius is therefore 2.06° . On Figure 8, we show where this radius falls on a plot of the surface density of galaxies. This r_{2t} estimate reasonably approximates the boundary of the group. It extends modestly outside the survey region.

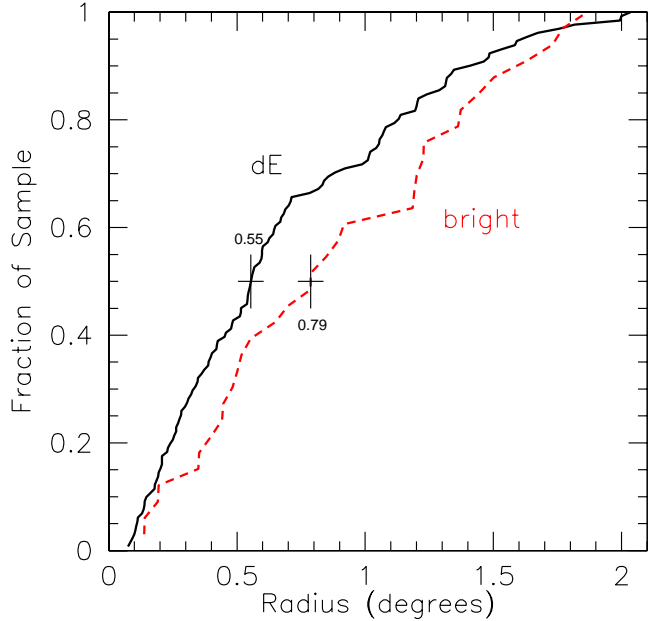


Figure 7. Cumulative radial distributions for the NGC 1407 Group. The solid curve at left shows the cumulative radial distribution of all (131) early types ($T \leq 1$) rated 1 or 2 fainter than $M_R = -17$. The dashed curve at the right shows the cumulative radial distribution of all (33) galaxies brighter than $M_R = -17$.

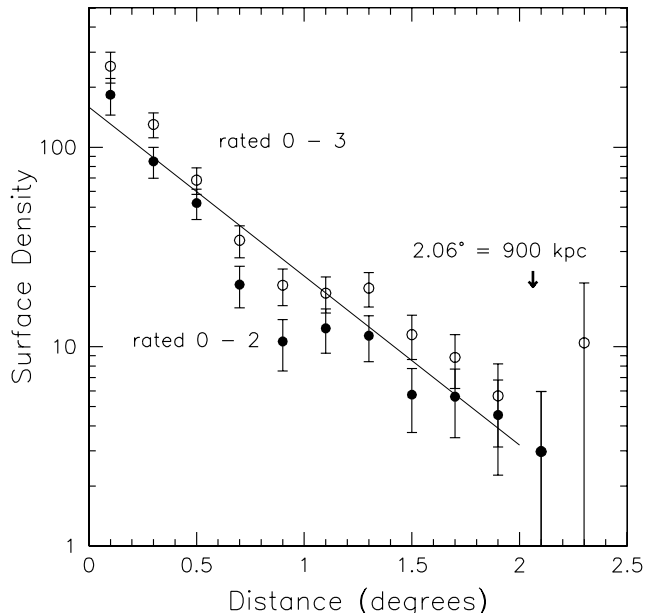


Figure 8. The variation of surface density of galaxies with radius. Filled symbols refer to systems with velocities or rated 1 and 2. Open symbols include the contribution from systems rated 3. Corrections for the restricted boundary of the survey are included. These are significant as radii greater than 1 degree and result in extremely large uncertainties for the 3 points at largest radii. The straight line represents a fit to the average of the pairs of points inside 2 degrees and has a slope of 0.85, implying a fall-off in the volume density with a slope of 1.85. The inferred radius of second turnaround is indicated at $2.06^\circ = 900$ kpc.

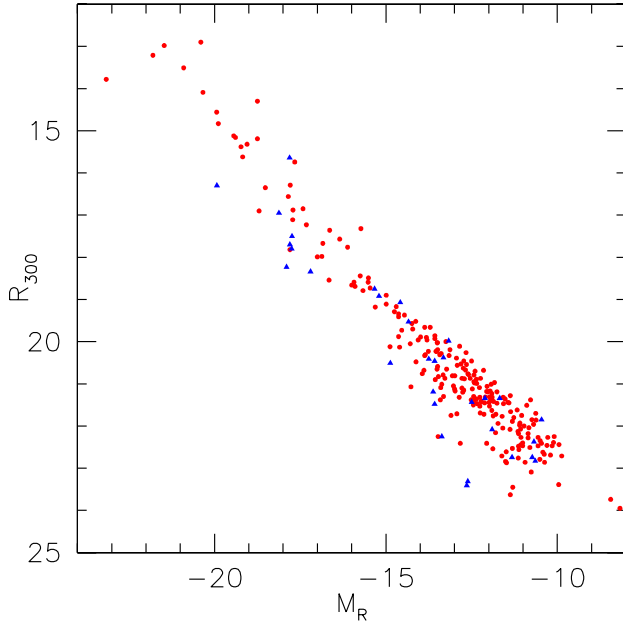


Figure 9. Central luminosity vs total luminosity. The central luminosity is the R -band flux measured within a 300 pc = 2.5 arcsec radius aperture. Types $T \leq 1$ and $T > 1$ are distinguished by circles and triangles respectively.

5.4 Galaxy scaling relations

The correlation between central surface brightness and absolute luminosity is shown in Figure 9. The measure of central surface brightness is R_{300} , the luminosity in a 300 pc = 2.5" radius aperture. The equivalent plot in MTT05 looks similar. For the galaxies in the sample, lower-luminosity galaxies have a systematically lower central surface brightness. Equivalently, as shown by MTT05, lower luminosity galaxies have lower surface brightnesses within the 'effective' radius containing half the light. Early type galaxies tend to lie above late type galaxies of the same magnitude. There is a hint of the gap at $R_{300} \sim 16$ seen in MTT05; galaxies with absolute magnitudes $M_R \sim -19$ have a tendency to avoid intermediate central surface brightnesses characterized by $R_{300} \sim 16$.

5.5 Normalization of the luminosity function

In TT02 and MTT05 we introduced a normalization of the luminosity function which enables us to compare results from different environments. The normalization is based on the number density of galaxies brighter than $M_R = -17$ at a fiducial radius of 200 kpc. For the NGC 1407 group the normalization is set at 34 galaxies/Mpc 2 (see Figure 10). The two sets of points plotted in Fig. 10 represent the radial distributions of bright galaxies and the equivalent distribution of the entire sample. The former is wanted to establish the luminosity function normalization just discussed. The latter is dominated by the dwarf population.

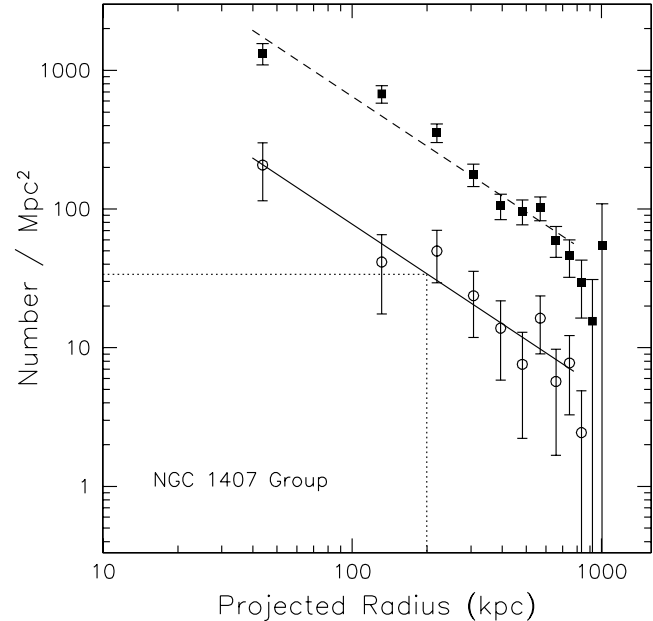


Figure 10. The radial distribution of bright galaxies and of all galaxies. The sample of galaxies with $M_R < -17$ is indicated by the open symbols and provide the surface density calibration at 200 kpc used to normalize the luminosity function. The filled symbols indicate the distribution of the entire sample. The solid line represents a fit to the bright sample and the dashed line is this same line shifted vertically so as to be appropriate to the entire sample.

5.6 Luminosity function

The group luminosity function is shown in Figure 11. The small filled and open circles show the range in possibilities if *no* objects rated 3 are members or *all* objects rated 3 are members, respectively. The squares with error bars are determined on the assumption that, brighter than -13.4 , 70% of the objects rated 3 are members, while fainter than -13.4 that 50% of early types are members but that none of later types are members. (the same rules determined for the NGC 5846 Group sample by MTT05). The turndown in the final two points is presumably due to incompleteness.

There is a dearth of luminous systems in the group after the brightest system, NGC 1407, at $4L^*$. The second brightest galaxy, NGC 1400, has a luminosity that is $\sim L^*$. The dwarf-to-giant ratio introduced by TT02 is defined as the number of galaxies with $-17 < M_R < -11$ over the number of galaxies with $M_R < -17$. For the NGC 1407 Group, that ratio is $200/31 = 6.5 \pm 1.3$ where the uncertainty includes estimates of the incompleteness near the $M_R = -11$ limit and membership uncertainties. This ratio is comparable with the value of 7.3 ± 0.7 found by MTT05 for the NGC 5846 Group but significantly larger than the ratio 2.6 ± 0.9 found for 4 other groups in the Local Supercluster by TT02 (Coma I, Leo, NGC 1023, Ursa Major).

In MTT05 and TT02 we attempted to fit separate luminosity functions to the bright and faint ends but such an exercise is not warranted here, because of small number statistics at the bright end. The straight line seen in Fig. 11 is a fit to the data with error bars. The fit conforms to the constraint of zero objects in the bin at $-23 < M_R < -22$

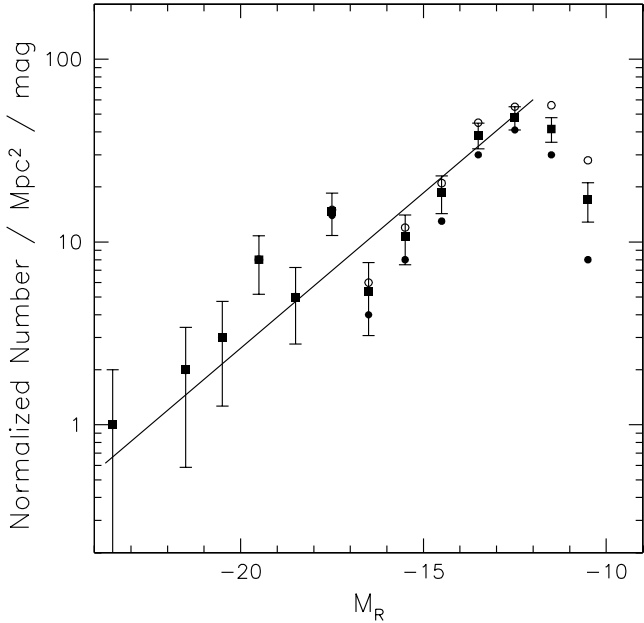


Figure 11. NGC 1407 Group luminosity function. Filled squares give normalized numbers per magnitude of galaxies confirmed as group members with velocities plus those with membership ratings 1 and 2, plus fractions of those with membership rating 3 as discussed in the text. Small filled circles: number with measured velocities or with membership ratings 1 and 2. Small open circles: also include galaxies with membership rating 3. The true luminosity function is expected to be bracketed by these extremes. Error bars reflect \sqrt{N} statistical variances. The straight line is a linear fit to the squares with error bars for $M_R < -12$. The slope is equivalent to a faint end Schechter function slope of $\alpha = -1.43 \pm 0.05$.

and then one (NGC 1407) in the next brighter bin. The slope of this line corresponds to the faint-end slope in the Schechter (1976) formulation of $\alpha = -1.43$. The usual exponential cutoff at the high luminosity end cannot be defined because there are so few objects above $M_R = -20$ and one very luminous system.

The discussion of the luminosity function is most meaningfully extended by amalgamating the NGC 1407 and (MTT05) NGC 5846 results. This is a particularly useful exercise because (a) the two groups are at similar distance, (b) observations of both were with the same CFHT camera for the same exposure times and reductions for both were analyzed with the same algorithms, and (c) the groups are very similar in dimensions, velocity dispersions (hence masses) and morphological compositions. The luminosity functions of the two groups are shown in Figure 12, separately through the small symbols and jointly through the large symbols. The two groups are seen to follow the same luminosity distribution without a significant offset in number surface density (after the normalization computed in the case of NGC 1407 using Fig. 10 and in the case of NGC 5846 using Fig. 12 in MTT05). The average luminosity function of the two groups is well-fit with a Schechter function (the solid line in Fig. 12) with a faint end slope $\alpha = -1.35$. The bright-end exponential cutoff is characterized by $M^* = -23.6$. This unusually bright cutoff can be attributed to the evolved states of the two groups. The dominant galaxies are unusually bright.

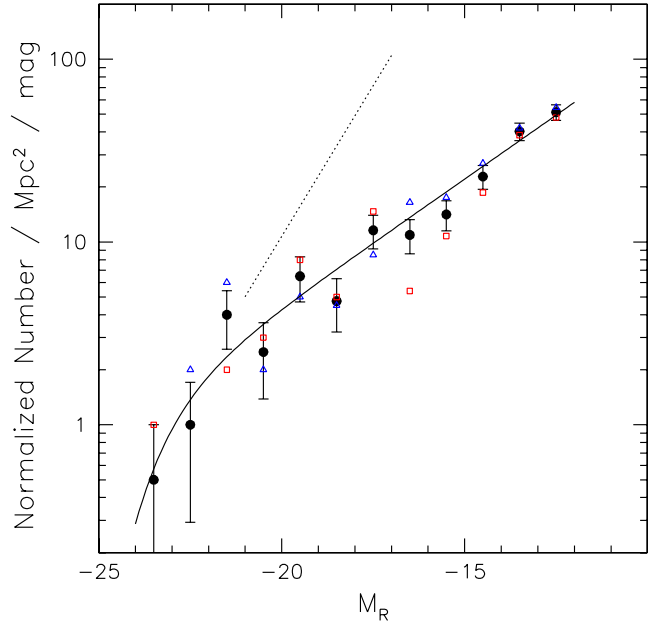


Figure 12. Luminosity function for the combined NGC 1407 and NGC 5846 groups. The large filled symbols with error bars show the combined data. The small squares and triangles give the data for NGC 1407 and NGC 5846 respectively. The solid curve illustrates a Schechter function fit to the combined data. The dotted line shows the slope anticipated for the mass function in a Λ CDM cosmology with arbitrary normalization.

The dotted line in Figure 12 demonstrates the slope of the mass function given by hierarchical clustering in the standard Λ CDM model. Clearly, the luminosity function is shallower.

Other comparisons with the combined NGC 1407/5846 luminosity function are made in Figure 13. The data defining luminosity functions found in the Virgo Cluster by TT02 and in the Ursa Major Cluster by Trentham et al. (2001) are superposed, scaled by the same normalization procedure. The curves are Schechter function fits characterized by a faint end slope parameter α and a bright end exponential break at M^* . The coupling between these parameters is seen in Figure 14. It is seen that the bright end break does not quite have 2σ significance for either the combined NGC 1407/5846 or U Ma samples. It may seem that the Virgo and NGC 1407/5846 samples have different slopes but the apparent difference is largely a consequence of the coupling between the parameters M^* and α and the clear requirement of a lower M^* with the Virgo data.

6 DISCUSSION AND CONCLUSION

The NGC 1407 Group is overwhelmingly an environment of galaxies deficient in cold gas and young stars. This point is emphasized by Figure 15, a plot updated from TT02 and MTT05. The environment is even more extreme in this respect than in the NGC 5846 Group or the core of the Virgo Cluster.

Here is a review of properties of the NGC 1407 Group that collectively suggest that the group is at an advanced state of dynamical evolution.

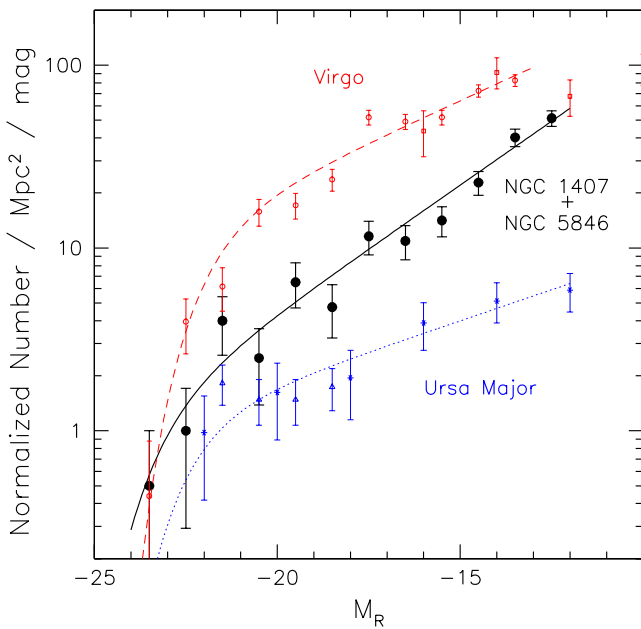


Figure 13. Luminosity function comparisons with the Virgo and Ursa Major clusters. The luminosity function found from the combined NGC 1407 and NGC 5846 data sets is compared with the luminosity function for the Virgo Cluster reported in TT02 and for the U Ma Cluster reported by Trentham et al (2001). Normalizations follow the same procedures. The solid curve is the Schechter function fit to the combined NGC 1407 and NGC 5846 material with Schechter function parameters $M^* = -23.6$ and $\alpha = -1.35$. The dashed curve shows the Schechter function fit to the Virgo data with $M^* = -22.2$ and $\alpha = -1.23$. The dotted curve shows such a fit to the U Ma data with $M^* = -22.7$ and $\alpha = -1.17$.

- The galaxy population is almost entirely Population II ellipsoids.
- The group is dominated by a single luminous galaxy 1.4^m brighter than the second brightest galaxy.
- That second brightest galaxy, NGC 1400, has an incredible differential motion of -1072 km s^{-1} with respect to the group mean.
- The bright galaxies are less concentrated to the center of the group than the dwarfs.

The NGC 1407 Group shares many of the properties of fossil groups (Ponman et al. 1994).

The depletion of intermediate luminosity systems in an evolved group is attributed to merging and subsequent growth of the central dominant galaxy (Jones et al. 2003). D’Onghia et al. (2005) have followed N-body/hydrodynamical models of clusters with similar masses of $\sim 10^{14} M_\odot$ and found a correlation between the magnitude interval between first and second brightest objects and the epoch when a group assembled 50% of its final mass. According to their simulations, a group with the properties found here would have assembled at $z \sim 0.8$.

We now show that this group possesses many dwarf galaxies, another similarity with fossil groups (Ponman et al. 1994; Mulchaey and Zabludoff 1999). This tells us that the physical process responsible for depleting the cluster of intermediate luminosity galaxies does not remove the entire dwarf galaxy population. This is the primary result of

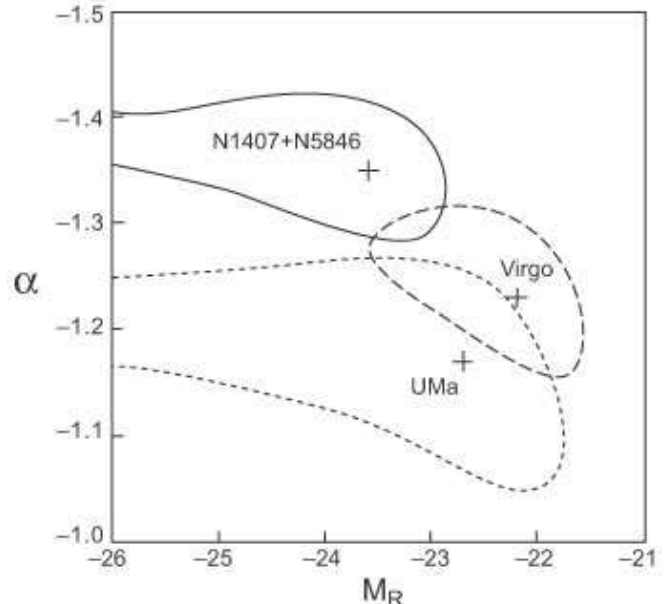


Figure 14. χ^2 constraints on parameters for Schechter function fits. Best χ^2 values lie at the crosses. Contours are 95% probability. Solid contour: combined NGC 1407/5846 groups. Dashed contour: Virgo Cluster. Dotted contour: Ursa Major Cluster. The contours open at high luminosity for NGC 1407/5846 and U Ma reveal that linear fits in these cases have χ^2 significance within 2σ of the best Schechter function fits.

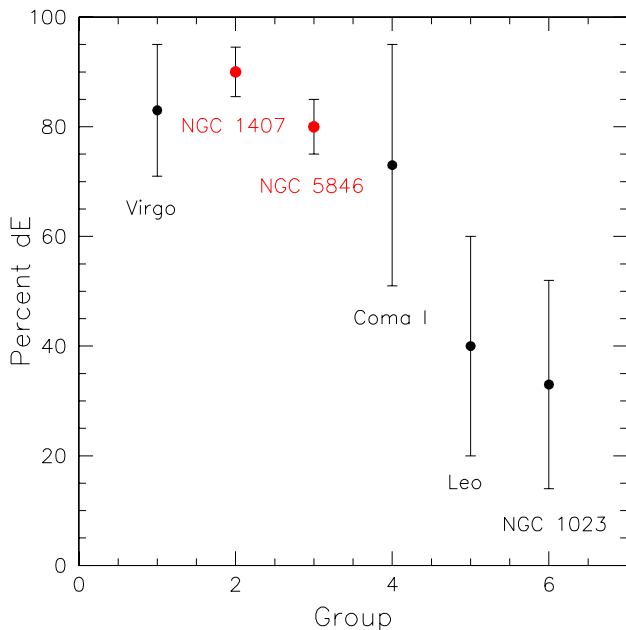


Figure 15. Percent of dwarfs that are early type. Galaxies with luminosities in the range $-17 < M_R < -11$ are split between early (dE, dE/I) and late types (VLSB, dI, dI/E). In the case of the NGC 1407 Group $90 \pm 5\%$ are early type. This fraction is compared with the values found by MTT05 and TT02 for other groups.

this paper. In the context of our wider study, the presence of a substantial dwarf elliptical population could well be a ubiquitous feature of dynamically evolved environments.

By comparison, the NGC 5846 Group studied by MTT05 appears to be younger. The two groups have comparable dimensions and velocity dispersions, hence total masses. However, the NGC 5846 group is a dumbbell system with two large ellipticals of comparable luminosity, each the center of an enhanced dwarf population. There are more intermediate luminosity galaxies in that group, with 5 L^* galaxies, including two spirals. The estimated total number of group members brighter than our survey limits are ~ 250 in both cases.

The large-scale environments of the two groups are somewhat different. The NGC 5846 group is a knot of early type galaxies in a filament that is otherwise low density and spiral rich. The spiral dominated filament probably provides the source for more recent infall into the NGC 5846 Group. By contrast, the NGC 1407 Group is adjacent other knots of early type galaxies. The larger region around NGC 1407 appears to be more dynamically evolved than the larger region around NGC 5846. In section 2.1 we inferred there is somewhat more than $10^{14} M_\odot$ in the Eridanus region identified by Tully (1988) as the 51-xx+4 association. The zero velocity or first turnaround surface at radius r_{1t} enclosing the bound region of this association can be estimated by scaling from the Local Group (Tully 2005):

$$r_{1t}^{Eri} \sim r_{1t}^{LG} (M^{Eri}/M^{LG})^{1/3} \sim 4 \text{ Mpc} \sim 9^\circ. \quad (6)$$

A circle of this radius projected onto the Eridanus region encloses most of the galaxies plotted in the left panel of Fig. 2. This region should collapse in on itself over the next Hubble time forming an entity comparable to the Fornax Cluster as seen today. The NGC 1407 Group (51-8 in the NBG catalog) appears at the moment to be the dominant mass component but the group around NGC 1395 and NGC 1398 is slightly more luminous and contains many more intermediate luminosity galaxies. The NGC 1407 group may be close to a fossil group today but it will be reinvigorated with new group members in the future.

The very high relative motion of NGC 1400 is a special feature of the NGC 1407 Group. The existence of a second highly blueshifted object, albeit a much less luminous system, shows that the motion of NGC 1400 is not an unique event. Both high velocity systems are very near to NGC 1407 and the center of the group. This lends additional support for the scenario advocated by Gould (1993): that there exists a very massive gravitational well around NGC 1407. In the context of the alternative model described earlier, the second blueshifted galaxy is a companion that is bound to NGC 1400 as both move past the group.

While there are certainly more dwarf galaxies in dense environments than in diffuse environments, there still appear to be fewer dwarf galaxies than low-mass dark matter subhalos (De Lucia et al. 2004). This tells us that whatever physical processes are responsible for the suppression of star formation in low-mass galaxies must operate less efficiently in clusters than in the field or that there are additional processes that operate in clusters or regions that evolve into clusters that cause the formation of dwarf galaxies. More definitive statements can be made when measurements for

a large sample of groups exhibiting a range of properties are available.

ACKNOWLEDGEMENTS

Support for RBT was provided by the US National Science Foundation award AST 03-07706. This research has made use of the NASA/IPAC Extragalactic Database (NED) which is operated by the Jet Propulsion Laboratory, Caltech, under agreement with the National Aeronautics and Space Association.

Imaging observations were with the the Canada-France-Hawaii Telescope (CFHT) facility MegaPrime/MegaCam, a joint project of CFHT and CEA/DAPNIA. CFHT is operated by the National Research Council of Canada, the Institute National des Sciences de l'Univers of the Centre National de la Recherche Scientifique of France, and the University of Hawaii. Spectroscopic observations were made at the W.M. Keck Observatory.

Images of the galaxies described in this paper can be obtained from the CFHT cutout service: <http://www.cadc.hia.nrc.ca/cadcbin/cfht/cfhtCutout>.

REFERENCES

Aune S. et al., 2003, SPIE, 4841, 513
 Bertschinger E., 1985, ApJS, 58, 39
 Beuing J., Dobereiner S., Böhringer H., Bender R., 1999, MNRAS, 302, 209
 Buote D. A., Fabian A. C., 1998, MNRAS, 296, 977
 Canizares C. R., Fabbiano G., Trinchier G., 1987, ApJ, 312, 503
 Cuillandre J.-C. et al. 2001, in Clowes R., Adamson A., Bromage G., eds, The New Era of Wide Field Astronomy, ASP Conference Series Vol. 232., ASP, San Francisco, p. 398
 Davis D. S., White R. E., 1996, ApJ, 470, 35
 D'Onghia E., Sommer-Larsen J., Romeo A. D., Burkert A., Pedersen K., Portinari L., Rasmussen J., 2005, ApJ, 630, L109
 De Lucia G., Kauffmann G., Springel V., White S. D. M., Lanzoni B., Stoehr F., Tormen G., Yoshida N., 2004, MNRAS, 348, 333
 Dressler L. L., Wilson A. S., 1985, ApJ, 291, 668
 Flint C., Metevier A. J., Bolte M., Mendes de Oliveira C., 2001, ApJS, 134, 53
 Gao L., De Lucia G., White S. D. M., Jenkins A., 2004, MNRAS, 352, L1
 Gould A., 1993, ApJ, 403, 37
 Jones D. H., Saunders W., Read M., Colless M., 2005, PASA, in press
 Jones L. R., Ponman T. J., Horton A., Babul A., Ebeling H., Burke D. J., 2003, MNRAS, 343, 627
 Khosroshahi H. G., Jones L. R., Ponman T. J., 2004, MNRAS, 349, 1240
 Klypin A., Kravtsov A.V., Valenzuela, O., Prada F., 1999, ApJ, 522, 82
 Mahdavi A., Trentham N., Tully R.B., 2005, AJ, 130, 1502 [MTT05]
 Mahdavi A., Geller M. J., 2001, ApJ, 554, 129
 Markevitch M., Forman W. R., Sarazin C. L., Vikhlinin A., 1998, ApJ, 503, 77
 Miles T. A., Raychaudhury S., Forbes D. A., Goudrooij P., Ponman T. J., Koshurina-Platais V., 2004, MNRAS, 355, 785
 Milgrom M., 1983, ApJ, 270, 371
 Moore B., Ghigna S., Governato F., Lake G., Quinn T., Stadel J., Tozzi P. 1999, ApJ, 524, L19
 Mulchaey J. S., Zabludoff A. I., 1999, ApJ, 514, 133

Oke J. B., 1995, PASP, 107, 375

Osmond J. P. F., Ponman T. J., 2004, MNRAS, 350, 1511

O'Sullivan E., Forbes D. A., Ponman T. J., 2001, MNRAS, 328, 461

Phillipps S., Drinkwater M. J., Gregg M. D., Jones J. B., 2001, ApJ, 560, 201

Ponman T. J., Allan D. J., Jones L. R., Merrifield M., McHardy I. M., Lehto H. J., Luppino G. A., 1994, Nat, 369, 462

Popesso P., Bohringer H., Romaniello M., Voges W., 2005, AJ, 133, 415

Quintana H., Fouqué P., Way M. J., 1994, A&A, 283, 722

Schechter, P.L., 1976, ApJ, 203, 297

Tonry J., Dressler A., Blakeslee J. P., Ajhar E. A., Fletcher A. B., Luppino G. A., Metzger M. R., Moore C. B., 2001, ApJ, 546, 681

Trentham N., 1997, MNRAS, 286, 133

Trentham N., Hodgkin S., 2002, MNRAS, 333, 423

Trentham N., Tully R. B., 2002, MNRAS, 335, 712 [TT02]

Trentham N., Tully R. B., Verheijen M. A. W., 2001, MNRAS, 325, 385 [TTV01]

Tully R. B., 1988, *Nearby Galaxies Catalog*, Cambridge University Press (NBG catalog)

Tully R. B., 2005, *Mass Scales and Shapes of Cosmological Structures*, (astro-ph/0509482)

Tully R. B., Verheijen M. A. W., Pierce M. J., Huang J.-S., Wainscoat R. J., 1996, AJ, 112, 2471

Zhang Z.-L., Xu H.-G., 2004, ChJAA, 4, 221